

ornl

OAK
RIDGE
NATIONAL
LABORATORY

UNION
CARBIDE

OPERATED BY
UNION CARBIDE CORPORATION
FOR THE UNITED STATES
DEPARTMENT OF ENERGY

OAK RIDGE NATIONAL LABORATORY LIBRARIES



3 4456 0555521 7

ORNL/TM-7043

ORCULT-I: A Loop Dynamics Simulator Program for the Core Flow Test Loop

S. J. Ball

OAK RIDGE NATIONAL LABORATORY

CENTRAL RESEARCH LIBRARY

CIRCULATION SECTION

4500N ROOM 175

LIBRARY LOAN COPY

DO NOT TRANSFER TO ANOTHER PERSON

If you wish someone else to see this
report, send in name with report and
the library will arrange a loan.

UCN-7969 13 9-771

Printed in the United States of America. Available from
National Technical Information Service
U.S. Department of Commerce
5285 Port Royal Road, Springfield, Virginia 22161
NTIS price codes—Printed Copy: A04; Microfiche A01

This report was prepared as an account of work sponsored by an agency of the United States Government. Neither the United States Government nor any agency thereof, nor any of their employees, makes any warranty, express or implied, or assumes any legal liability or responsibility for the accuracy, completeness, or usefulness of any information, apparatus, product, or process disclosed, or represents that its use would not infringe privately owned rights. Reference herein to any specific commercial product, process, or service by trade name, trademark, manufacturer, or otherwise, does not necessarily constitute or imply its endorsement, recommendation, or favoring by the United States Government or any agency thereof. The views and opinions of authors expressed herein do not necessarily state or reflect those of the United States Government or any agency thereof.

Contract No. W-7405-eng-26

INSTRUMENTATION AND CONTROLS DIVISION

ORCULT-I: A LOOP DYNAMICS SIMULATOR PROGRAM
FOR THE CORE FLOW TEST LOOP

S. J. Ball

NOTICE This document contains information of a preliminary nature.
It is subject to revision or correction and therefore does not represent a
final report.

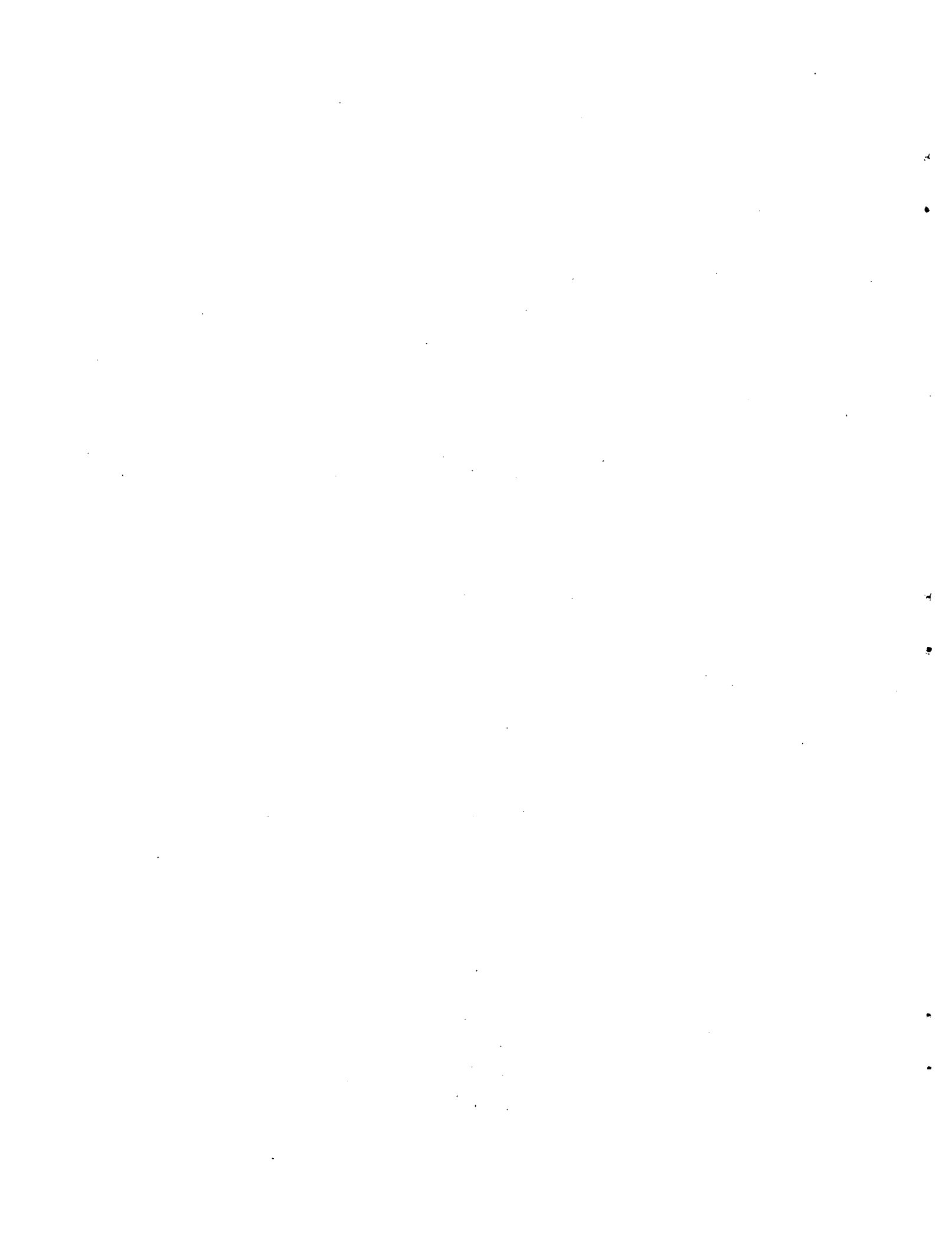
Date Published - February 1980

Prepared by the
OAK RIDGE NATIONAL LABORATORY
Oak Ridge, Tennessee 37830
operated by
UNION CARBIDE CORPORATION
for the
DEPARTMENT OF ENERGY

OAK RIDGE NATIONAL LABORATORY LIBRARIES



3 4456 0555521 7



ORCULT-I: A Loop Dynamics Simulator Program
for the Core Flow Test Loop

S. J. Ball
Oak Ridge National Laboratory
Oak Ridge, Tennessee 37830

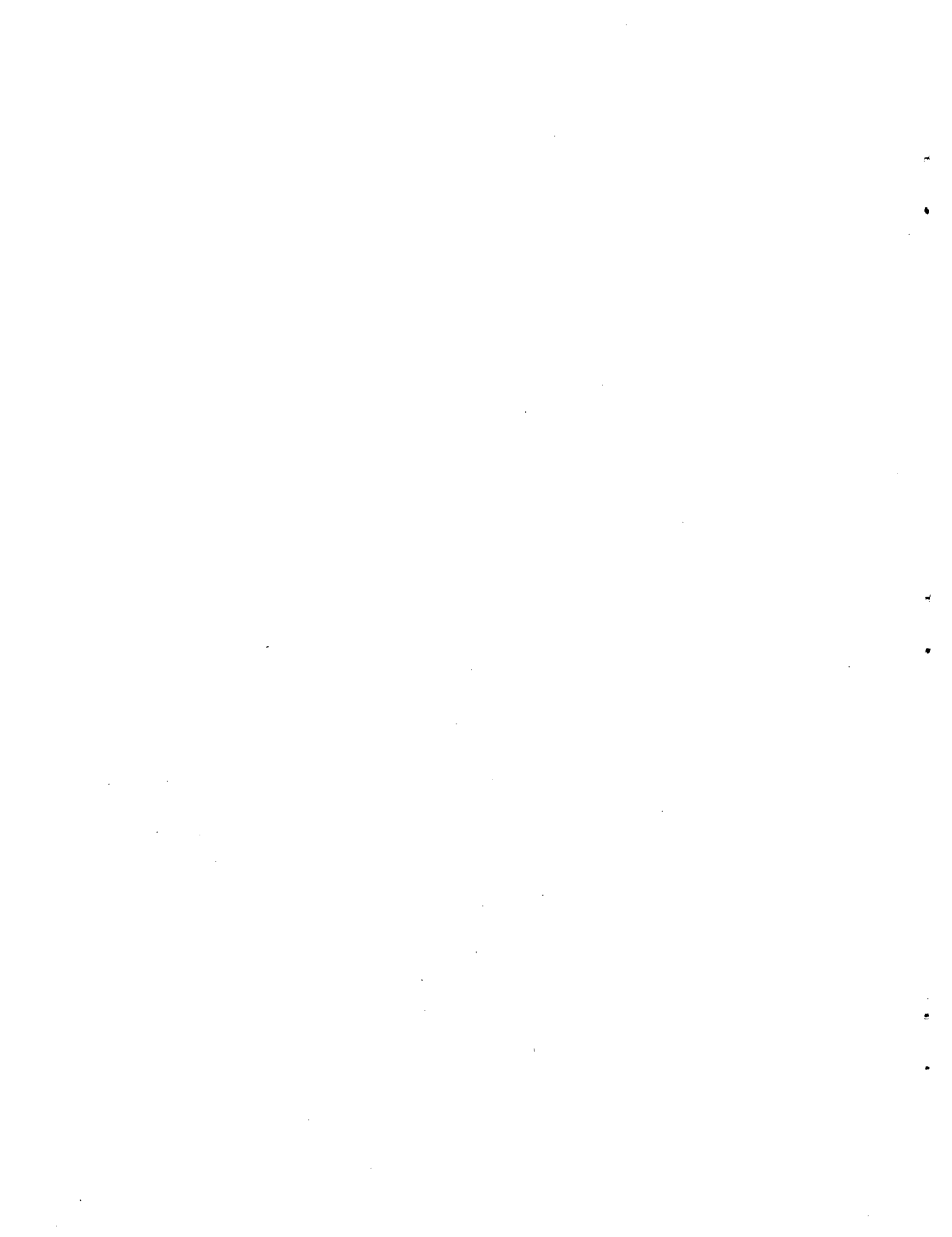
HIGHLIGHTS

A digital simulation program, ORCULT-I, was developed to predict both the steady-state and transient behavior of the core flow test loop (CFTL). ORCULT has been used to answer design questions concerning loop configurations, operating modes, bundle tests, and postulated loop-accident conditions. The CFTL is a thermal-hydraulic and structural test vehicle for performance evaluations of Gas-Cooled Fast-Breeder Reactor (GCFR) fuel-rod bundle designs.

Rod bundle behavior is approximated in ORCULT by a model of a single average rod and flow channel. Spatial variations are accounted for by dividing the rod into six axial sections. Radial temperature distributions within the rod may be calculated as an option, but radial flow and temperature variations within the bundle are not accounted for. Fine-structure models represent the loop heat exchangers and piping, and the performance maps for the helium circulators are included. When the loop helium inventory is changed, such as when a simulated depressurization accident is studied, mass and internal energy balance equations are used in a two-node approximation. The loop control systems are also simulated.

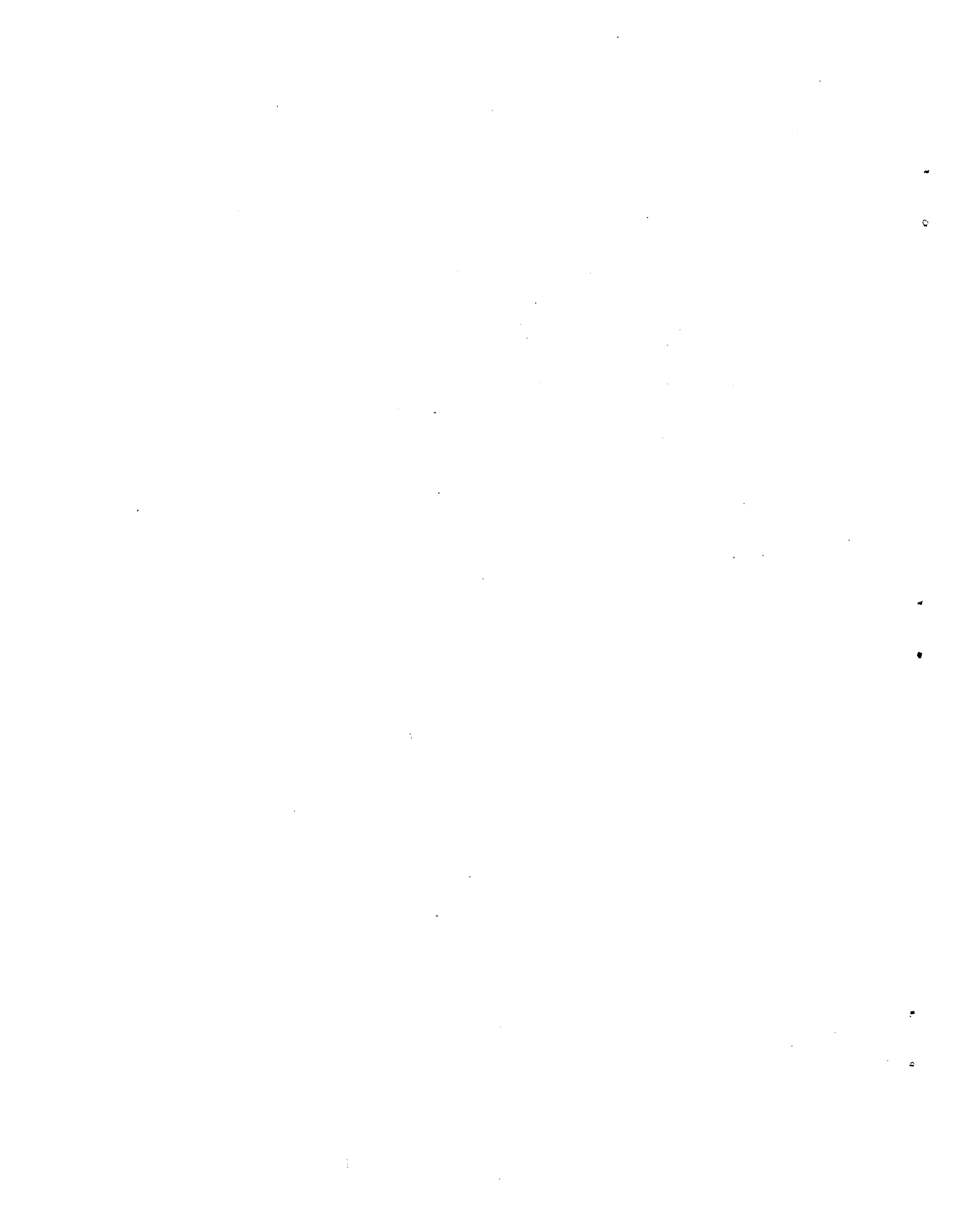
The status, capabilities, and limitations of ORCULT are described, and several sample transients are shown which demonstrate characteristics of CFTL behavior. The appendix of the report includes derivations of the model equations used in ORCULT. Certain simulation techniques described may be generally useful. The code is written in CSMP-III, an IBM simulation language. The ORCULT code will assist in fine-tuning the proposed loop control and safety systems and in loop test planning and evaluations.

November 1979



CONTENTS

	<u>Page</u>
1. Introduction	1
2. Description of Loop and Component Simulations	1
2.1 Loop Description	1
2.2 Test Section Simulation	3
2.3 Heat Exchanger Simulation	5
2.4 Circulators and Flow Equations	7
2.5 Piping and Filter Simulation	7
2.6 Control Systems Simulation	7
3. Description of ORCULT Versions and Capabilities	11
4. Example Transients	12
5. Conclusions	17
6. Appendix - Derivation of ORCULT Models	18
6.1 Test Section	18
6.2 Heat Exchangers	27
6.3 Circulator and Loop Flow Equations	32
6.4 Pipe Models	46
6.5 Controller Model	51
References	52



1. INTRODUCTION

The purpose of this report is to describe the status, capabilities, and limitations of the ORCULT (Oak Ridge CFTL Underrated Loop Transient) code. Also, this report describes various simulation techniques which may be generally useful and some sample transients which demonstrate certain characteristics of the CFTL dynamic behavior.

The ORCULT code utilizes the IBM simulation language CSMP-III,¹ which enables efficient conversion from the nonlinear differential equations that describe the system to an operating program.

ORCULT appears in several versions, each designed to meet a particular project need. Because of the structure of the CSMP language, it is usually more efficient to generate a new version of the program that is designed for a specific task than it is to try to modify a single program's input data. Hence, there are different ORCULT programs for studying design basis depressurization accidents (DBDAs), blower coast-downs, loop control problems, and steady state operation and control problems.

The author thanks W. A. Hartman, M. Hatta (IHI-Japan), and A. D. McNutt for their assistance and advice on many of the model development problems.

2. DESCRIPTION OF LOOP AND COMPONENT SIMULATIONS

2.1 Loop Description

The CFTL is a thermal-hydraulic and structural test vehicle for evaluating the performance of Gas-Cooled Fast Breeder Reactor (GCFR) core designs. A flow diagram is shown in Fig. 1. Helium gas at pressures up to 9 MPa (1300 psi) and at mass flows up to 3.18 kg/s (7 lb_m/s) is driven by three hermetic circulators connected in series to maximize the head. The gas passes through a test section containing up to 91 electrically heated fuel rod simulators (FRSs). The nominal value of the test section inlet temperature is 350°C (662°F), and at a rated power of 28 kW/rod, the rod bundle outlet temperature is ~566°C

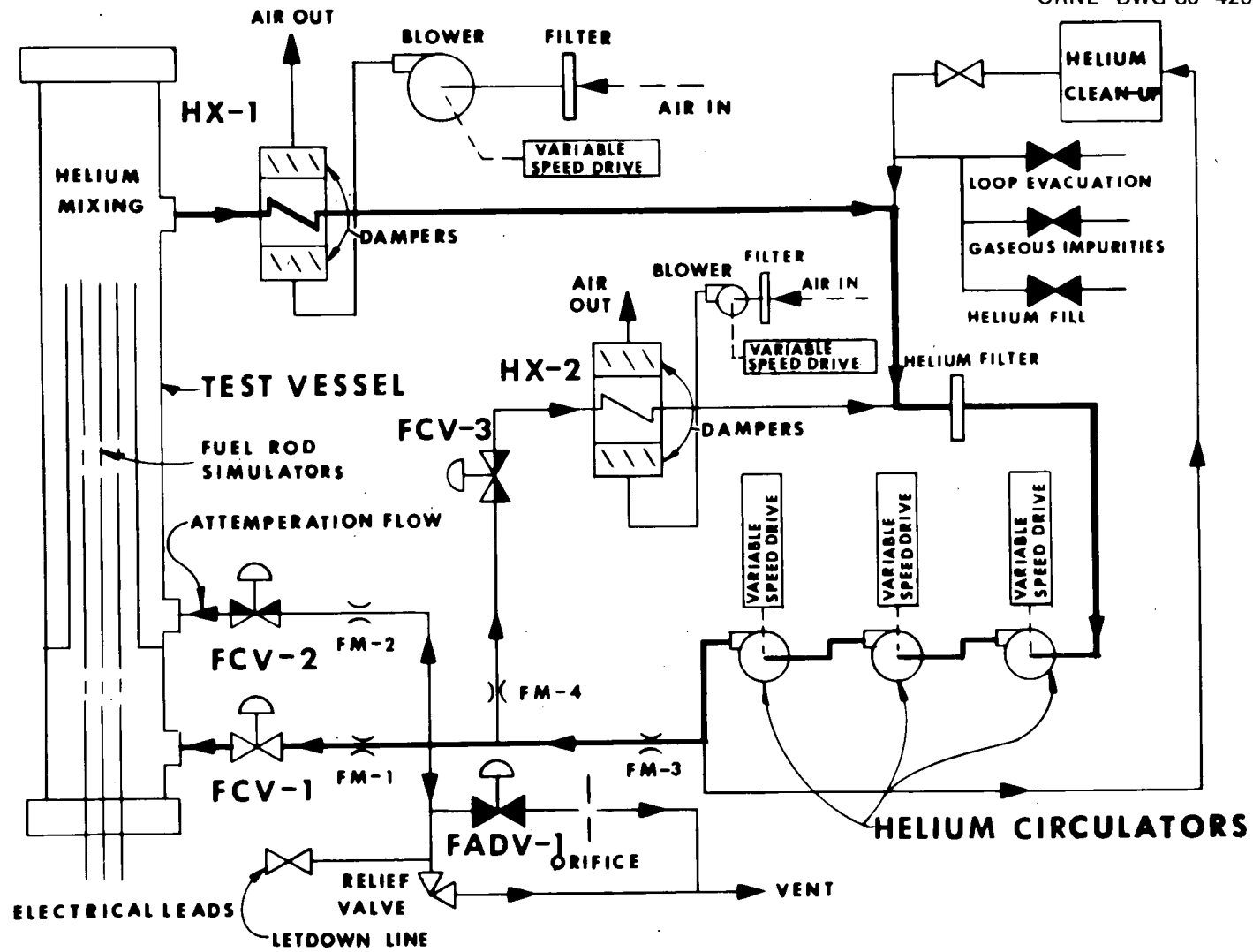


Fig. 1. CFTL flow diagram.

(1051°F) before attemperation. The loop accommodates steady-state bundle powers of up to 45 kW/rod at 2.8 kg/s (6.14 lb_m/s) and simulates postulated GCFR accident conditions for powers of up to 38 kW/rod. Flow in the test bundle is upflow to correspond to a recent change in GCFR core design. Mixing of the bundle outlet and attemperator flows occurs in the upper (outlet) plenum of the test section and in a short, heavy-duty section of downstream piping equipped with a mixer. The helium enters the tube side of a 4-MW air-blast heat exchanger (HX-1), a filter, and then the circulators. For Stage 2 operation, there will be a bypass line with a second heat exchanger (HX-2, 0.4 MW) to help absorb the higher power and flow transients. In an early stage (Stage 1), the smaller heat exchanger is omitted. The return line to the test section will have a branch to contain the exhaust valve used for DBDA simulation.

2.2 Test Section Simulation

A drawing of the test section (Fig. 2) shows the inlet plenum flow distributor, (unheated) inlet blanket region, heated fuel section, outlet blanket, and the outlet mixing region. The transient thermal behavior of the rod bundle is represented in ORCULT by a single average rod and flow channel. Spatial variations are normally modeled by dividing the rod into six axial sections, one each for the blankets and four for the active fuel, with a single (radial) node for each section. A five-radial-node-per-section model is alternatively used for cases in which greater FRS detail is desired, but tests have shown that the predicted external loop performance is independent of the assumed core node structure.

The test section simulation makes use of a CSMP "MACRO" (similar to a subroutine) developed for a one-radial-node rod section. The MACRO takes, as inputs, the initial mean solid temperature, electrical power input, inlet gas temperature, solid-to-clad heat transfer coefficient, gas-to-solid time constant, and dimensionless coefficient which is a measure of the total heat transfer rate between the solid and gas for a given gas flow. The MACRO outputs are the average solid temperature, clad temperature, and gas outlet temperature.

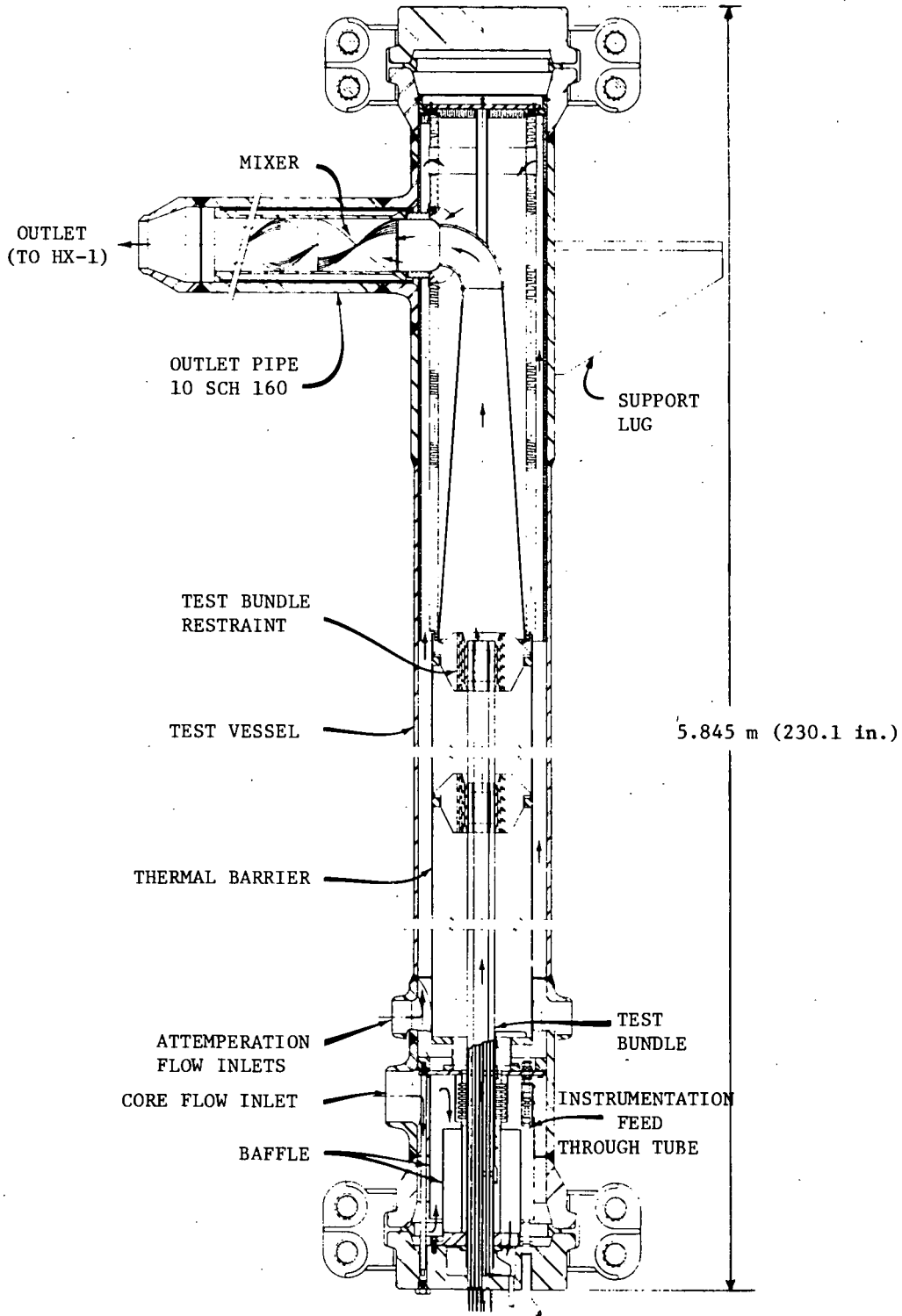


Fig. 2. CFTL test section details.

Because of the difference in thermal properties between a GCFR fuel rod and an FRS, the at-power heat storage in the FRS is considerably less. (Since UO_2 is a relatively poor conductor, the internal temperature of the fuel rod is much greater than that of the FRS.) Since an objective of the CFTL is to simulate the GCFR rod-cladding behavior during transients, differences in heat storage will be accounted for by appropriate modification of the transient power inputs to the FRS.² Thus, in ORCULT runs that simulate transients such as a DBDA or scram, a GCFR fuel rod simulation is used with the prescribed reactor power input and the implicit assumption that the electrical power to the FRS has been properly modified. For CFTL studies of loop-related transients such as loss of bundle power, the FRS model is used.

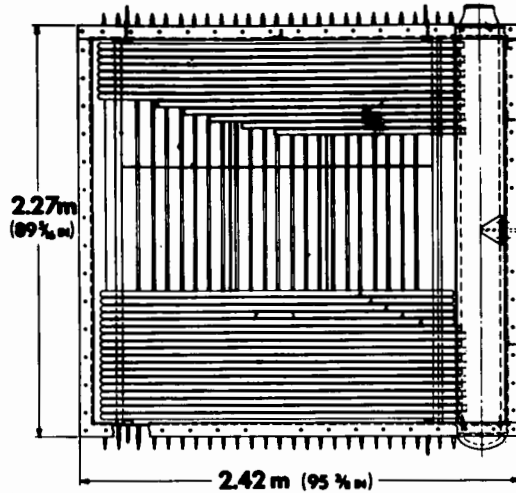
Derivations of the FRS and fuel rod equations are given in Appendix 6.1.

2.3 Heat Exchanger Simulation

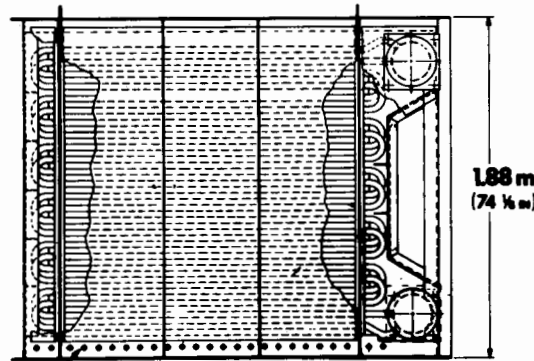
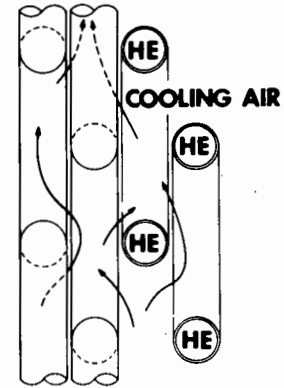
Details of the 4-MW main heat exchanger are shown in Fig. 3. The design of the 0.4-MW bypass line heat exchanger is very similar. The heat exchangers are of the crossflow/counterflow, tube-and-shell type, and are designed to operate over wide ranges of power and helium (tube side) and air (shell side) flows. Special versions of the ORCULT code were used to estimate the transient thermal stresses in the HX-1 and to provide information for the design of the helium inlet header.

ORCULT modeling of the heat exchangers was based on techniques developed previously for gas-cooled heat exchanger dynamics.³ Special provisions were required to accommodate the wide ranges of helium and air flows, and, as a result, HX-1 was modeled by a 12-node and HX-2 by a 7-node approximation. The usual ORCULT loop dynamics programs assume that the cooling air flow is a controlled input; however, a special version was created to calculate HX-1 cooling via natural convection air flow.

Details of the heat exchanger model and equation development are given in Appendix 6.2.

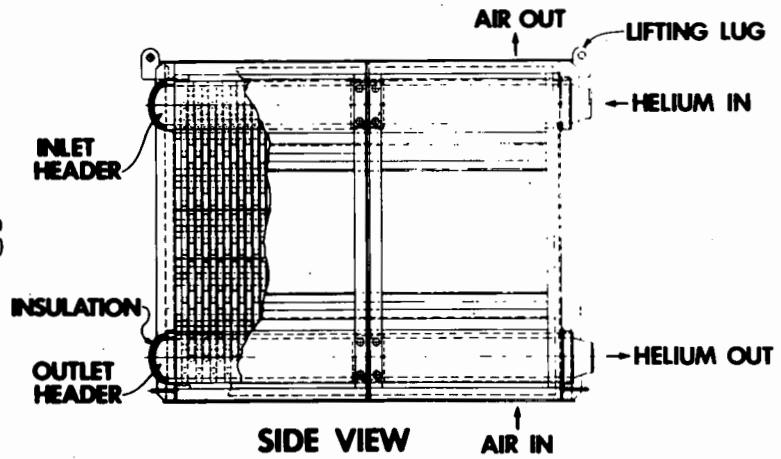


TOP VIEW



FRONT VIEW

ELECTRICAL
HEATERS



SIDE VIEW

Fig. 3. HX-1 details.

2.4 Circulators and Flow Equations

Details of an individual CFTL circulator are shown in Fig. 4, and a composite three-circulator performance map as supplied by the vendor is shown in Fig. 5. Recasting the performance parameters in terms of a normalized $\Delta P/\rho N^2$ vs a normalized $W/\rho N$ permits transforming the entire map into a single-valued function which is readily approximated by a quadratic equation (Fig. 6).^{*} Further assumption of square-law flow vs pressure drops in the loop would allow an explicit calculation of total circulator flow by solving a single quadratic equation. Although several of the loop components do not have a $\Delta P = KW^2/\rho$ relationship, by continuous appropriate variations of the resistance parameter K, the quadratic solution can still be used (and it is in ORCULT).

CFTL simulations for which the helium mass in the loop is unchanged use an algebraic (instantaneous) solution to find the flows throughout the entire loop. For other cases, such as the DBDA, a two-node mass balance approximation is used. More recently, the internal energy equations were included in order to approximate the effects of expansion cooling during DBDAs.

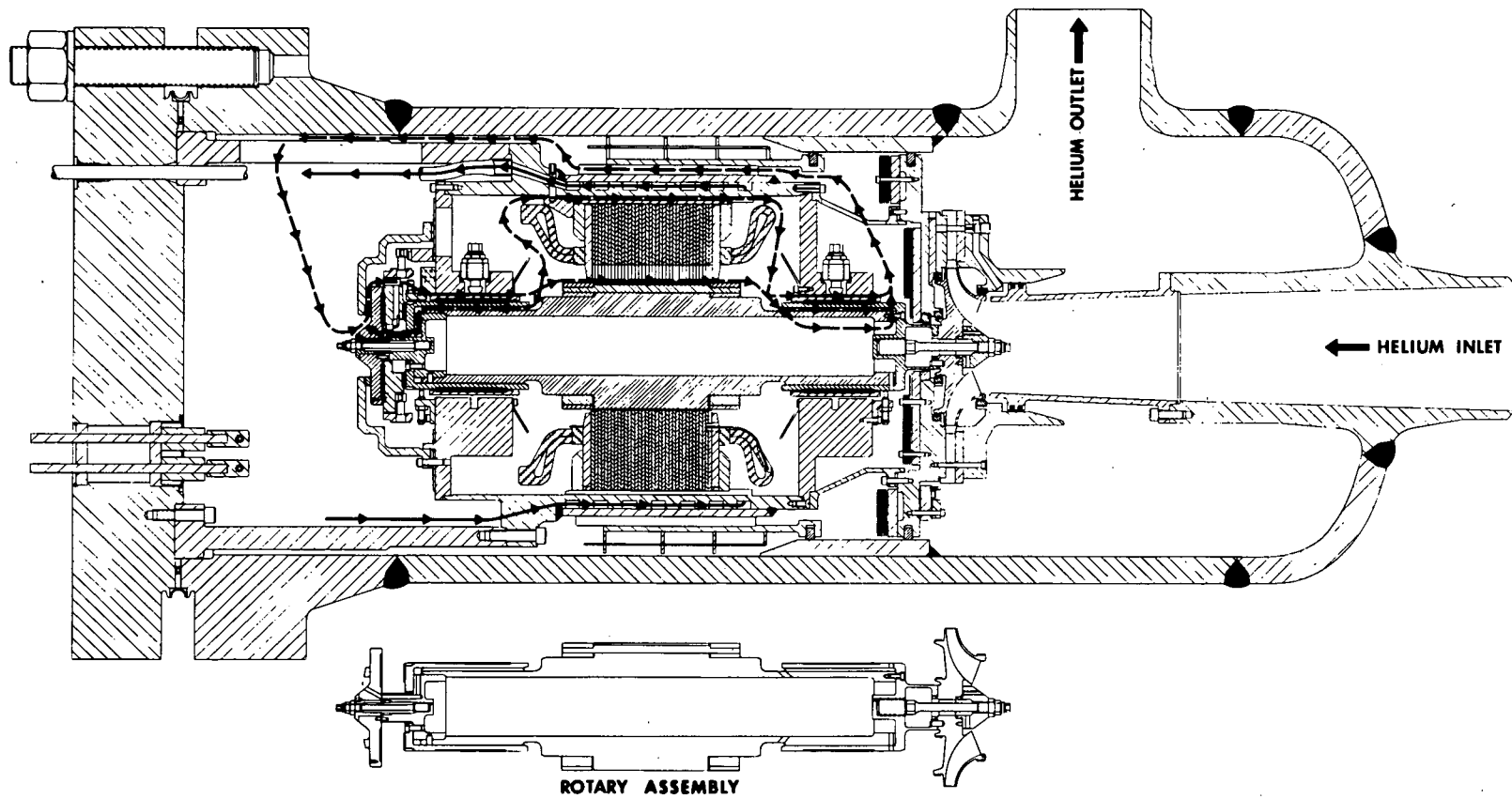
2.5 Piping and Filter Simulation

The thermal inertia of the interconnecting piping and the filter is useful in mitigating the effects of large temperature transients, especially for cases in which the total loop mass flow is reduced significantly. The derivation of the method used to simulate piping lags is given in Appendix 6.4. The equations for the fine-structure thermal gradient analysis (used to determine transient thermal stresses) are also given.

2.6 Control Systems Simulation

One use of the ORCULT code is that it can aid the design of control systems by testing proposed designs. The main objectives of the control system are to supply the test bundle with power and helium at the pressure,

^{*}See Appendix 6.3 for definitions and more details.



COOLING FLOW DIAGRAM
HELIUM CIRCULATOR FOR
GCFR CORE FLOW TEST LOOP (CFTL)
(BY MECHANICAL TECHNOLOGY INC.)

Fig. 4. Circulator details.

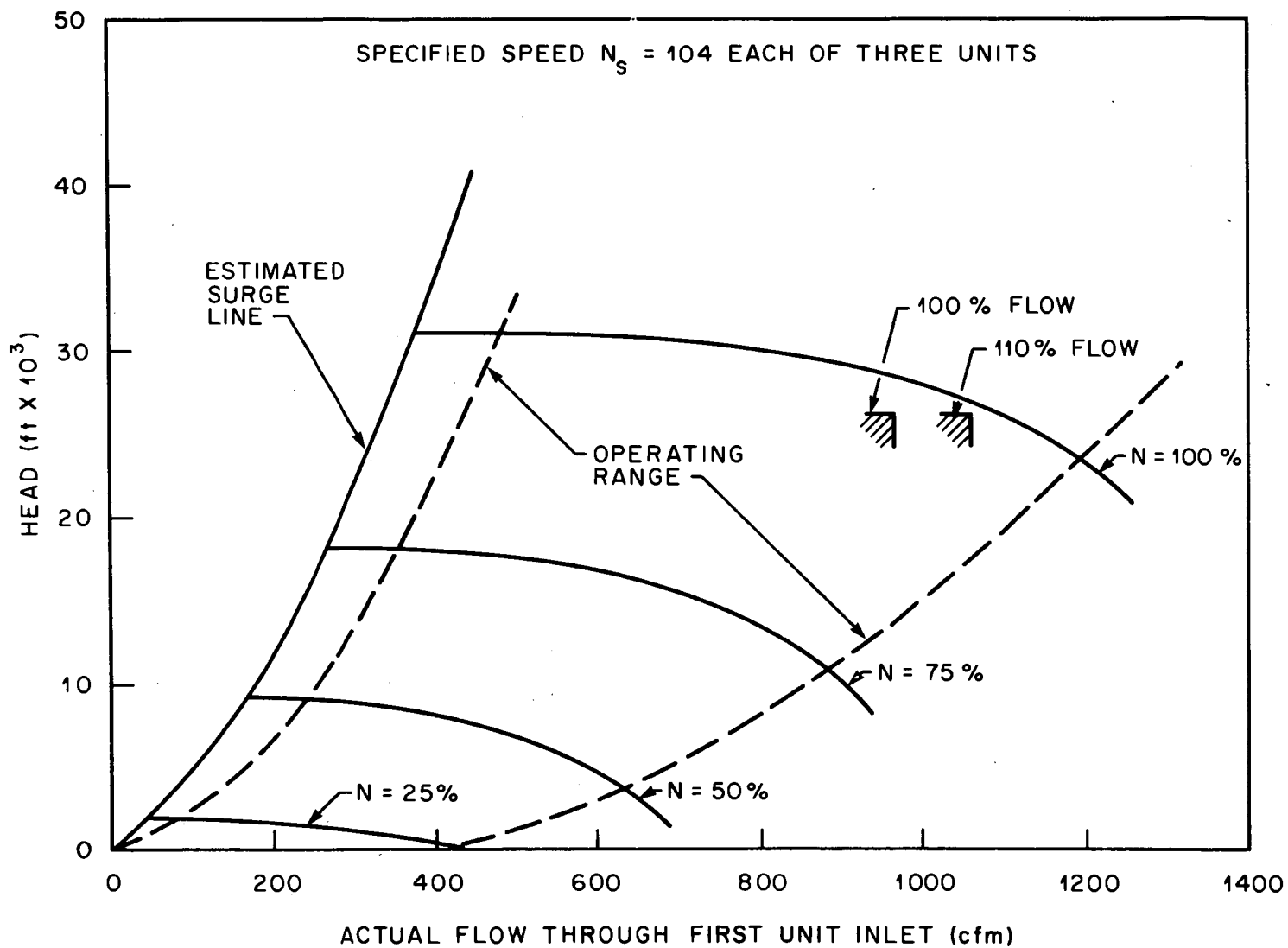


Fig. 5. Composite three-circulator performance map.

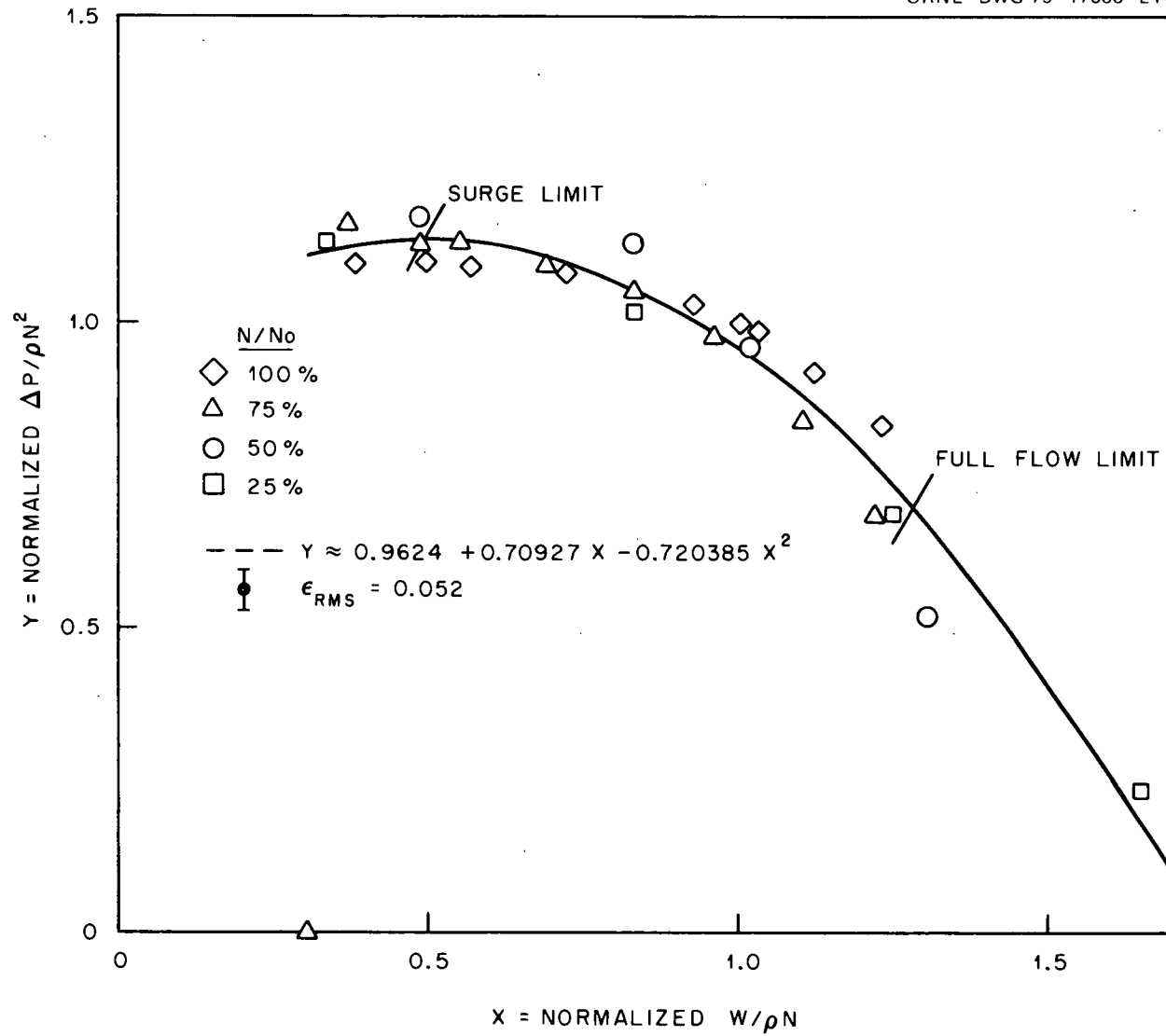


Fig. 6. Normalized circulator performance map.

temperature, and flow conditions prescribed by the test program, and, at the same time, to minimize the shock imposed on all the components in the external loop. Specifically, high-temperature cycling at the HX-1 helium inlet and elevated and rapid temperature changes at the circulators are to be minimized. HX-1 inlet transients are controlled by programmed changes of the attemperator flow. The circulators are protected by action of the HX-1 control system, which maintains a fixed helium outlet temperature by varying the cooling air flow. Anticipation signals from the helium inlet temperature and flow are also used to vary the cooling air flow. In the simulator, a CSMP MACRO is used for a standard proportional-integral-derivative (PID) controller, and a derivation of the PID MACRO is in Appendix 6.5.

3. DESCRIPTION OF ORCULT VERSIONS AND CAPABILITIES

Because of the structure of the CSMP-III simulation language, it is often more convenient and efficient to create several versions of a simulation than to run different loop configurations and types of transients by changing the input data. Consequently, the ORCULT code exists in several versions, each of which is updated as design changes are made on the loop. These versions are summarized in Table 1.

Table 1. Versions of the ORCULT code

<u>Version</u>	<u>Comments</u>
1. Depressurization (dynamic)	HX-2 model is excluded
2. Constant helium inventory (dynamic)	Mass and internal energy balance equations excluded
HX-2 included	Reference design loop (stage 2)
HX-2 excluded	For stage 1 design studies
3. Steady state	Dynamic equations omitted

The dynamic version which accommodates depressurization transients includes a two-node approximation for both the mass and internal energy balances. The HX-2 model is omitted because it is planned to cut off

its helium flow during depressurization tests. To study the loop dynamics for constant helium inventory, one version without the HX-2 model is used for stage 1 design studies; the other version has the full complement of equipment for studying the reference design. For all dynamics versions, either the FRS or the fuel rod model is used, depending on the purpose of the run. Input data changes are also used to convert to different-size bundles.

The steady-state version of ORCULT is used mainly for sizing valves, noting the operating ranges for valve coefficients (c_v), blower speeds, and heat exchanger coolant conditions and the need for pipe line heaters. Eventually, it may be useful (converted to a DAS on-line program) to help operators set up test conditions and to detect loop component anomalies.

To date, the model for natural convection of coolant air in the HX-1 has been run as a separate calculation, but the model will be combined with the total-loop ORCULTS when detailed control system tuning studies are done.

4. EXAMPLE TRANSIENTS

Two examples are presented to show some of the capabilities and output features of the ORCULT code, as well as to indicate some of the basic dynamic characteristics of the CFTL.

The first example is a DBDA transient for the case of a 91-rod bundle with an initial power level of 28 kW/rod and an assumed blowdown sequence corresponding to a 0.048 m^2 (75 in.²) hole in a GCFR. Conservative assumptions of decay heat, bundle flow, and loop pressure vs time were taken from ref. 4. Steam-driven circulator coastdown characteristics were used in the reference calculation. (Updated inputs representing electric-driven circulator characteristics will be substituted when they become available.) As mentioned previously, the test bundle simulation makes use of the fuel rod (vs FRS) model along with the estimated reactor decay heat curve. This assumes that in the CFTL test a modified power curve has been input into the FRSs to compensate for the lower FRS heat storage.

The results of the simulation are shown in Figs. 7 and 8. One concern in the design of the valve control system is whether the test bundle control valve (FCV1) and the attenuator line control valve (FCV2) will be regulated in such a way that the prescribed test section flow transient will be obtained and, at the same time, that the circulators' nominal flow and ΔP operating range will not be exceeded. In this case (Fig. 7), the values of c_v for FCV1 vs time were calculated as those required to give the prescribed flow, while FCV2 was manipulated to keep the circulators near the midpoint of their desired operating range. The valve manipulations required a wide c_v range. The discontinuity at about 85 s into the transient ($t = \sim 97$) was due to the simulation of the shutoff of the main GCFR circulators, with a subsequent startup of the core auxiliary cooling system (CACS). To maintain the desired circulator operating point, FCV2 opened quickly to its maximum c_v value (~ 110). The calculation indicates that the circulators were kept well within a normal and desirable operating range.

For the same DBDA transient, Fig. 8 shows how effectively the mixer and other piping between the test section and the HX-1 absorbed the high-temperature transient, thus sparing the HX-1 much of the thermal stress it would have experienced otherwise. Other cases in which detailed temperature gradients in the HX-1 inlet header and tubing were obtained showed that the HX-1 could withstand DBDA transients without exceeding allowable stress limits.

The purpose of the second example transient was to study a postulated loop accident, that is, to determine how fast the circulator inlet temperature would rise if all the cooling air to the HX-1 were cut off and if both the circulator speed and the test-section power were left on full (Fig. 9). The results show that an interlock which would trip both the circulator power and the test bundle power on high HX-1 helium outlet temperature appeared to be required. The results indicate that a trip signal for an HX-1 outlet temperature 11°C (20°F) above normal should be sufficient as a backup for a normal trip signal from an inadvertent loss of HX-1 cooling. However, since HX-1 cooling is essentially "off" for many prescribed operating conditions, it may be advisable to have a

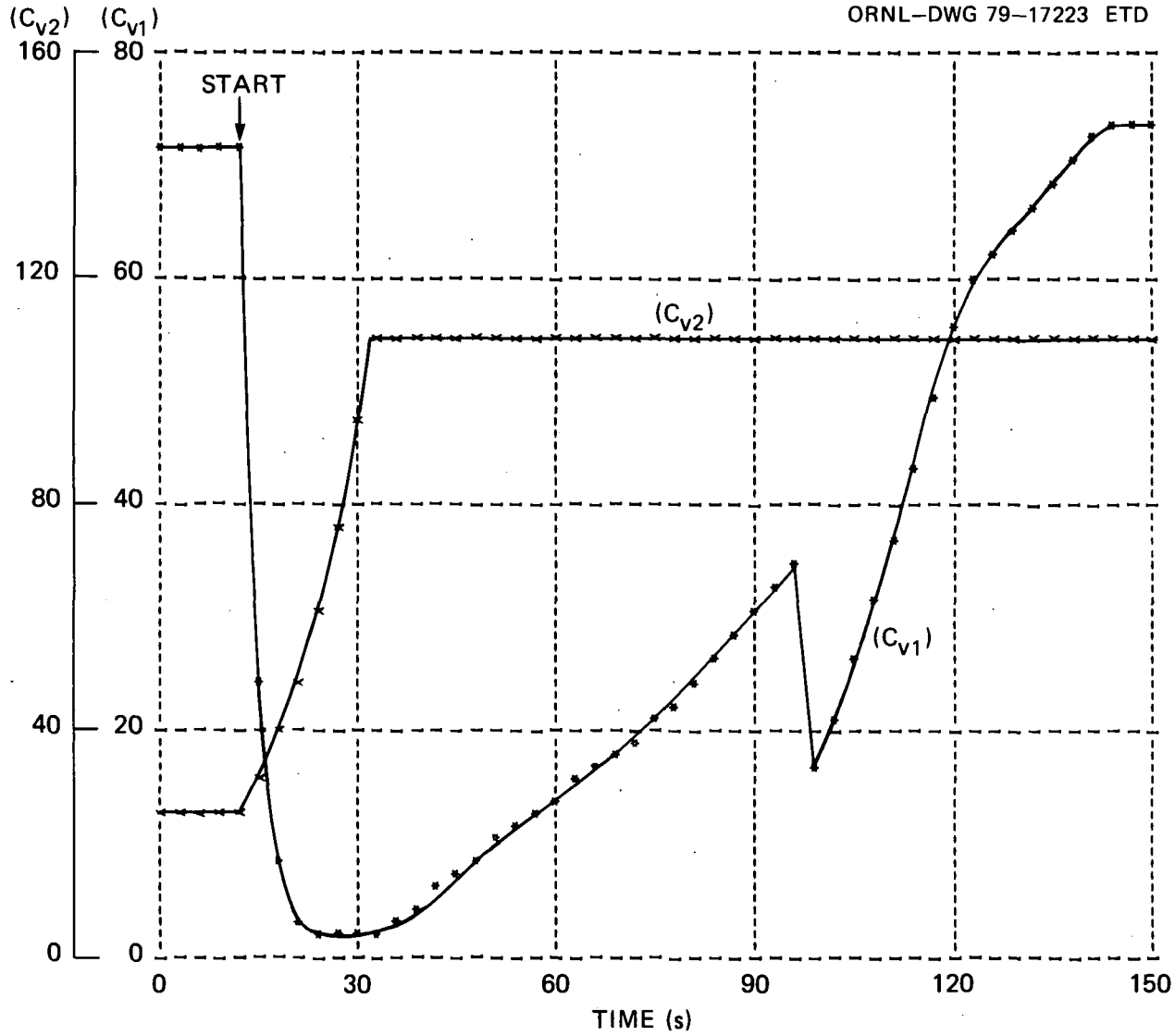


Fig. 7. Control valve manipulations during a DBDA.

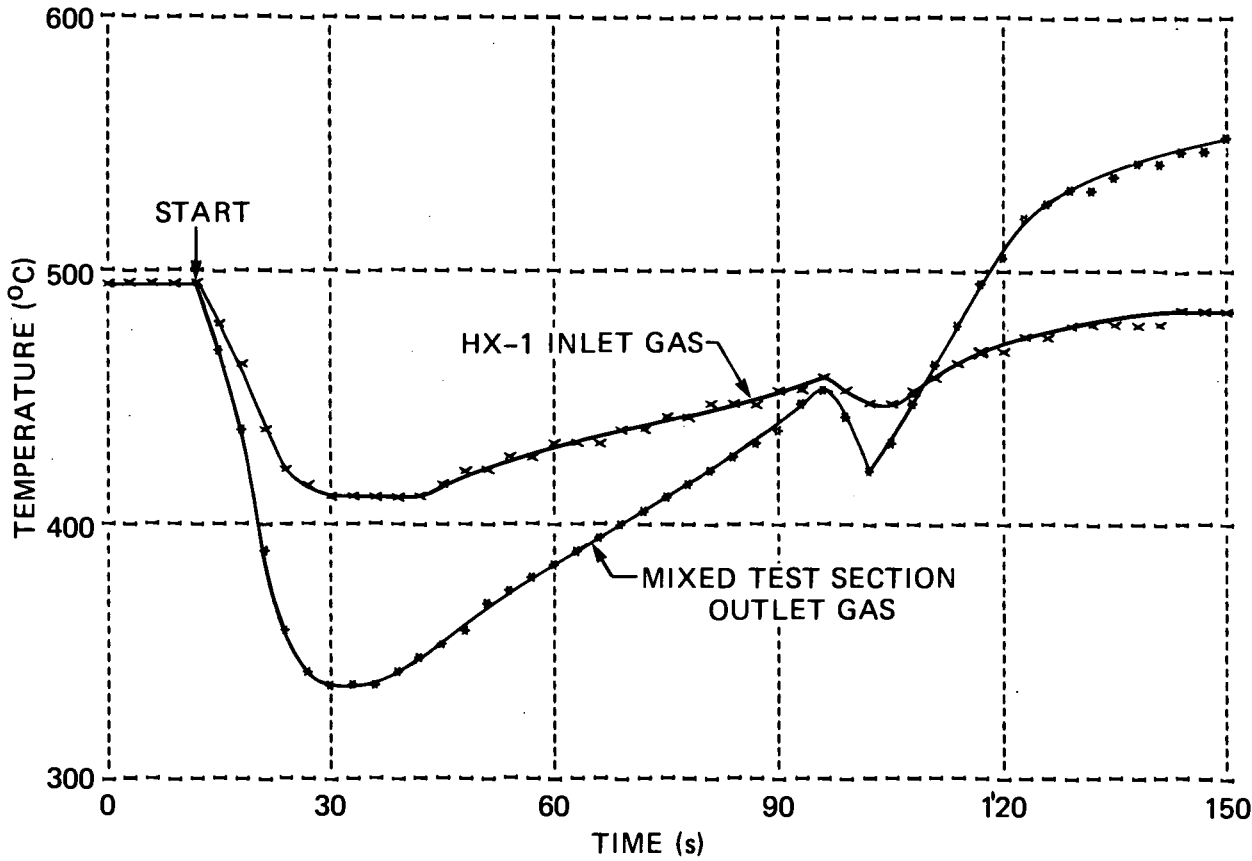


Fig. 8. Loop temperature responses to a DBDA.

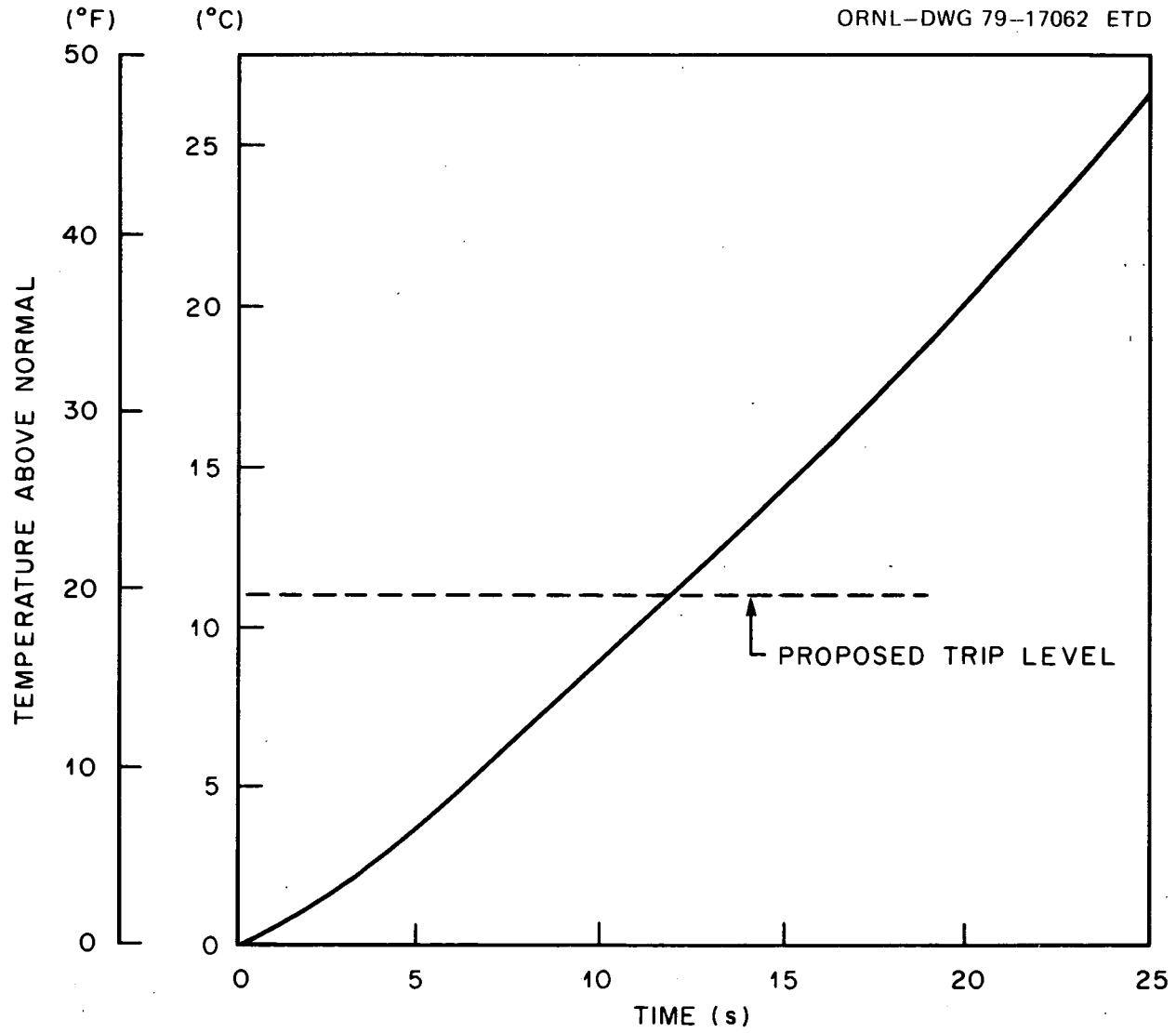


Fig. 9. Response of circulator inlet temperature after loss of HX-1 coolant.

high temperature trip in the helium outlet line as the only signal for protecting against loss of HX-1 cooling.

5. CONCLUSIONS

The ORCULT code has been used in all phases of the CFTL loop design, and it will be used to answer new questions about loop operation and to assist loop operations by making pretest predictions of loop performance for specific transient tests. In this latter usage, it will be important to use loop performance data to verify and upgrade the models used in ORCULT. Because the CFTL bundle design is still evolving, especially after recent changes in FRS design and loop flow direction, ORCULT will require more modification and development.

Planned model improvements include upgraded correlations used for bundle heat transfer and pressure drop as results from more extensive bundle analyses become available. Also needing more study is the accuracy of approximating the internal energy redistribution in the loop during DBDAs with a given number of nodes. Then, too, should a need arise for further studies of low-flow conditions, applications of the present correlation values to laminar regimes and incorporation of the bouyancy terms in the primary loop flow equations would be required.

The major, near-future use seen for the ORCULT code is that it will aid in the fine-tuning of the proposed control and safety systems for the bundle and the loop.

6. APPENDIX: DERIVATION OF ORCULT MODELS

6.1 Test Section

As noted in Sect. 2.2, the ORCULT simulation of a test bundle uses either an FRS model or a fuel rod model, depending on the purpose of the simulation. In all cases, a single average rod and coolant path model is used to characterize the bundle. The model uses one axial section, each, for the inlet and outlet blanket regions and divides the heated region into four axial sections. While some simulation runs have utilized an FRS model with five radial nodes per section, most have used a model with a single average radial node since the difference has little effect on the results for the external loop.

6.1.1 FRS conduction model

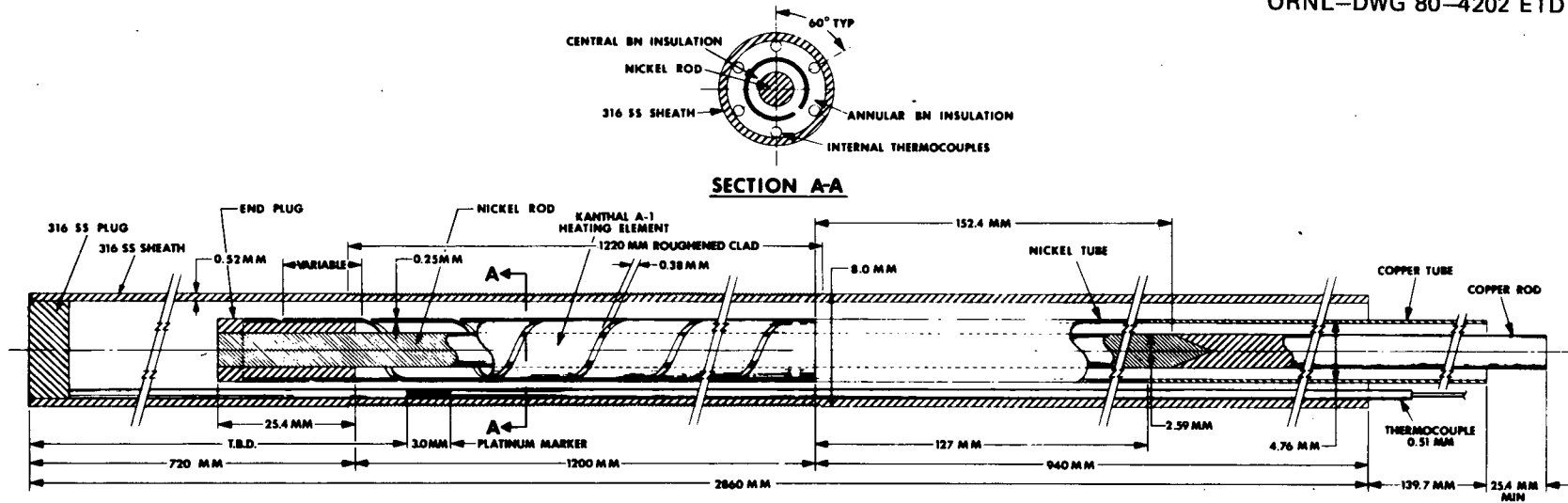
Since the FRS internals consist of a variety of components (Fig. 10), the approach used to generate a one-node model is to calculate an average heat-capacity-weighted temperature rise for a given input power. The equivalent one-node model equation is

$$(MC_p)_F \frac{d\bar{T}_F}{dt} = \left(\frac{\overline{kA}}{\Delta r} \right) (T_S - \bar{T}_F) + Q, \quad (1)$$

where

$$\begin{aligned} (MC_p)_F &= \text{composite heat capacity, Btu/}^\circ\text{F,} \\ \bar{T}_F &= \text{rod (FRS) average temperature, }^\circ\text{F,} \\ \left(\frac{\overline{kA}}{\Delta r} \right) &= \text{average heat conductance within the FRS, Btu s}^{-1}\text{ }^\circ\text{F}^{-1}, \\ T_S &= \text{rod surface temperature, }^\circ\text{F,} \\ Q &= \text{rod heat input, Btu/s.} \end{aligned}$$

From the steady-state solution of Eq. (1), the equivalent conductance term can be derived. The key parameters used in deriving the FRS model are shown in Table 2.



GCFR-CORE FLOW TEST LOOP (CFTL)
 FUEL ROD SIMULATOR

Fig. 10. FRS internal details.

Table 2. FRS conduction model parameters

	<u>Return rod</u>	<u>Inner Insulation</u>	<u>Heating Element</u>	<u>Outer Insulation</u>	<u>Sheath</u>
Material	Nickel	Boron Nitride	Kanthal	Boron Nitride	316 SS
ID, in.	-	0.102	0.1675	0.1875	0.275
OD, in.	0.102	0.1675	0.1875	0.275	0.315
Density, lb/in. ³	0.369	0.0722	0.774	0.0722	0.288
Specific heat, Btu lb ⁻¹ °F ⁻¹	0.071	0.418	0.037	0.418	0.15
Conductivity, Btu hr ⁻¹ ft ⁻¹ °F ⁻¹	58	13.5	40	13.5	14.5
Heat capacity (heated section), Btu/°F	0.0101	0.0198	0.00528	0.04531	0.03783
Full-power average temperature drop across element, °F*	1.36	5.78	10.58	262.16	48.62
Mean temperature rise referenced to sheath outer surface temperature, °F*	327.82	324.25	317.76	179.70	24.31

*For a 38 kW/rod, with 3% of the total power generated in the central return rod and 1% in the upper blanket, and 1200-mm heated section.

To determine the radial temperature profiles in the FRS elements (Fig. 11), the following equations were used:

1. Solid cylinder (nickel return rod)

a. Centerline temperature:

$$\theta(0) = \frac{qr^2}{4k}, \quad (2)$$

where

$\theta(0)$ = centerline temperature referenced to surface temperature, °F,

q = heat generation rate per unit volume, $\text{Btu s}^{-1}\text{in.}^{-3}$,

r = cylinder radius, in.,

k = conductivity, $\text{Btu s}^{-1}\text{in.}^{-1}\text{°F}^{-1}$.

b. Mean temperature:

$$\bar{\theta} = \theta(0)/2, \quad (3)$$

where

$\bar{\theta}$ = mean cylinder temperature referenced to surface temperature, °F.

2. Hollow cylinder with external heat source* (inner and outer insulation, heating element, and cladding)

a. Temperature drop:

$$\Delta\theta = \frac{Q \ln(d_o/d_i)}{2\pi kL}, \quad (4)$$

where

$\Delta\theta$ = radial temperature drop across cylinder, °F,

Q = heat flow through cylinder, Btu/s,

d_o, d_i = outer and inner diameters of cylinders, in.,

L = length of cylinder, in.

*external means generated within the "hollow space".

ORNL-DWG 80-4203 ETD

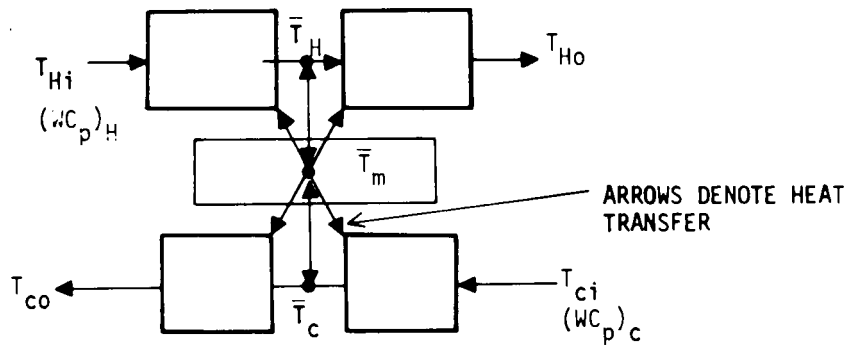


Fig. 11. Typical heat exchanger section model.

b. Mean temperature:

$$\bar{\theta} = \Delta\theta/2 , \quad (5)$$

where

$\bar{\theta}$ = mean hollow cylinder temperature rise referenced to outer surface temperature, °F.

3. Slab with internal heat generation (heating element approximated by slab geometry)

a. Temperature drop (with one side "insulated"):

$$\theta(0) = \frac{qr^2}{2k} , \quad (6)$$

where

$\theta(0)$ = "insulated," or inner surface, temperature referenced to other surface temperature, °F,

r = ribbon thickness, in.

b. Mean temperature:

$$\bar{\theta} = \frac{2}{3} \theta(0) , \quad (7)$$

where

$\bar{\theta}$ = mean slab temperature rise referenced to outer surface temperature, °F.

Based on the data in Table 2, the typical heated section of an FRS with a 38-kW input has a mean temperature rise (referenced to the outside surface temperature) of 173°F and stores 20.5 Btu; with no cooling, its mean temperature would increase at a rate of 301°F/s.

Because the fuel rod axial power distribution is a chopped cosine, the heated-length sections have different power inputs:

$$\text{Normalized } \bar{Q} = \int_{-1}^1 \cos 1.049y \cdot dy = 1.653 . \quad (8)$$

With the heated length divided into four sections, the two middle sections are each

$$\bar{Q}_m = \int_0^{0.5} \cos 1.049y \, dy = 0.4774 , \quad (9)$$

and the end sections are each

$$\bar{Q}_E = \int_{0.5}^1 \cos 1.049y \, dy = 0.3490 . \quad (10)$$

The fractions of total power in each middle section are $0.4774/1.653 = 0.289$, and in each end section are $0.349/1.653 = 0.211$.

6.1.2 FRS-to-coolant heat transfer model

The preceding section analyzed the mean FRS temperature relative to its surface temperature. To relate these two temperatures to the helium coolant temperatures, we define two parameters: the "section length," n ; and the fuel (or FRS) time constant based on surface temperature being the driving function, τ_S :

$$n = \frac{hA}{(WC)_{p \text{ gas}}} , \quad (11)$$

and

$$\tau_S = \frac{(MC)_F}{hA} , \quad (12)$$

where

- h = gas-to-surface heat transfer coefficient,
Btu s⁻¹ in⁻² °F⁻¹,
- A = outside surface area of rod in axial section, in.²,
- $(WC)_{p \text{ gas}}$ = mass flow rate of gas (per rod), lb/s, times specific
heat of helium gas (1.242), Btu lb⁻¹ °F⁻¹,
- τ_S = rod time constant referenced to sheath, s,
- $(MC)_F$ = heat capacity of rod axial section, Btu/°F.

A factor which accounts for the varying ratio between the temperature drop from mean fuel-to-sheath and sheath-to-mean gas is

$$\text{TAUF} \equiv \frac{\bar{T}_F - T_S}{T_S - \bar{T}_G} . \quad (13)$$

Since at steady state

$$Q = hA (T_S - \bar{T}_G) = \text{FB} (MC_p)_F (\bar{T}_F - T_S) , \quad (14)$$

then

$$\text{TAUF} = \frac{1}{\tau_S \cdot \text{FB}} , \quad (15)$$

where

$$\begin{aligned} \bar{T}_G &= \text{mean gas temperature in axial section, } ^\circ\text{F}, \\ Q &= \text{total heat generated in rod in axial section, Btu/s}, \\ \text{FB} &= \left(\frac{\overline{KA}}{\Delta r}\right) / (MC_p)_F, \text{ s}^{-1} \text{ [see Eq. (1)].} \end{aligned}$$

Since the gas holdup times are small compared to the thermal time constants, an instantaneous (algebraic) energy balance relationship is valid:

$$(\overline{WC}_p)_{\text{gas}} (T_{Go} - T_{Gi}) = hA (T_S - \bar{T}_G) ,$$

or

$$T_{Go} - T_{Gi} = n (T_S - \bar{T}_G) , \quad (16)$$

where

$$T_{Gi}, T_{Go} = \text{axial section inlet and outlet gas temperatures, } ^\circ\text{F}.$$

The FRS model is divided into small-enough sections so that an arithmetic-mean temperature difference approximation gives accurate results:

$$\bar{T}_G = 0.5 (T_{Gi} + T_{Go}) . \quad (17)$$

Combining Eqs. (16) and (17) gives

$$\bar{T}_G = \frac{T_{Gi} + n T_S / 2}{1.0 + n/2} . \quad (18)$$

Solving for \bar{T}_G in terms of the state variable \bar{T}_F by combining Eqs. (13) and (18) gives

$$\bar{T}_G = \frac{T_{Gi} + \frac{n/2}{1 + \tau_{AUF}} \bar{T}_F}{1.0 + n/2 \left(\frac{1}{1 + \tau_{AUF}} \right)} \quad (19)$$

The FRS model MACRO in ORCULT solves the differential equation for the mean rod temperature, Eq. (1); the equation for the mean gas temperature, Eq. (19); for gas outlet temperature, from Eq. (17); and for the surface temperature, from Eq. (18).

The latest project estimates⁵ of the overall bundle heat transfer coefficients are (at rated flow) $h \approx 1800 \text{ Btu hr}^{-1} \text{ ft}^{-2} \text{ } ^\circ\text{F}^{-1}$ for the roughened sections and $h \approx 1000 \text{ Btu hr}^{-1} \text{ ft}^{-2} \text{ } ^\circ\text{F}^{-1}$ for the smooth sections, with h varying as the 0.8 power of flow in both cases. "Rated flows" for the various bundles are defined as

37-rod fuel - 860 g/s (1.896 lb/s),
 91-rod fuel - 2115 g/s (4.663 lb/s),
 61-rod blanket - 1600 g/s (3.53 lb/s).

Values of the model parameters n and τ_S were calculated for each of the bundles and are tabulated as functions of bundle mass flow in Table 3.

Table 3. FRS-to-coolant heat transfer model parameters

	37-rod FRS (Fuel)	91-rod FRS (Fuel)	61-rod FRS (Blanket)
Rod time constant τ_S , s			
heated section	1.216 $W^{-0.8^a}$	2.499 $W^{-0.8}$	3.595 $W^{-0.8}$
blanket section	2.189 $W^{-0.8}$	4.498 $W^{-0.8}$	3.595 $W^{-0.8}$
Rod section length n			
1/4 heated section	0.7246 $W^{-0.2}$	0.8671 $W^{-0.2}$	0.4041 $W^{-0.2}$
inlet blanket section	1.26 $W^{-0.2}$	1.511 $W^{-0.2}$	1.266 $W^{-0.2}$
outlet blanket section	0.9654 $W^{-0.2}$	1.158 $W^{-0.2}$	0.97 $W^{-0.2}$

^a W is the total bundle mass flow, lb/s.

6.1.3 Fuel rod model

The approach used to generate a one-radial-node fuel rod model is similar to that used for the FRS, and, as a result, some interesting comparisons can be made between the predictions of dynamic behavior. The same model equation is used [Eq. (1)], and, for consistency, 1% of the reference power input (38 kW) is assumed to be generated outside the heated section. The pertinent model parameters for the fuel rod are summarized in Table 4.

One important assumption in deriving an effective conductance term for the fuel rod is the fuel-to-sheath gap ΔT . A pessimistically high value of 500°F was obtained from the GCFR preliminary safety information document. Both because of the large gap resistance and the relatively low conductivity of the UO_2 fuel, the mean temperature rise (1039°F) and heat storage (131 Btu) at reference power conditions are much larger in the fuel rod than in the FRS. The ratio of the two stored heat terms for these models is 6.4, which means that a FRS power control program will have to add significantly more heat to the FRS during a transient to make the FRS sheath temperatures respond like fuel rod sheath temperatures.

6.2 Heat Exchangers

6.2.1 Dynamics

Modeling of the dynamics of gas-to-gas heat exchangers follows the development noted in ref. 3. A typical section of a heat exchanger model is shown in Fig. 11.

The energy equation for the tube metal \bar{T}_m is

$$\frac{d\bar{T}_m}{dt} = \frac{1}{\tau_H} (\bar{T}_H - \bar{T}_m) + \frac{1}{\tau_c} (\bar{T}_c - \bar{T}_m), \quad (20)$$

where \bar{T}_H is the hot fluid mean temperature, °R; τ_H is the hot-side tube time constant $\left[= (MC_p)_m / (hA)_H \right]$, s; and τ_c is the cold-side tube time constant $\left[= (MC_p)_m / (hA)_c \right]$, s. Constants τ_c and τ_H are independent of length but vary as h changes with flow rate.

Table 4. Fuel rod model parameters

Fuel

Material	UO ₂
OD, in.	0.275
Density, lb/in. ³	0.361
Specific heat, Btu lb ⁻¹ °F ⁻¹	0.078
Conductivity, Btu hr ⁻¹ ft ⁻¹ °F ⁻¹	1.4
Heat capacity of heated section, Btu/°F	0.0882
Full-power average temperature rise, surface to centerline, °F	1854
Mean temperature rise referenced to sheath outer surface temperature, °F	1476

Gap

Full-power ΔT , °F	500
----------------------------	-----

Sheath

(same as FRS,
Table 2)

Rod Time Constant τ_G , s

37-rod heated section	1.2952 W ^{-0.8^a}
blanket section	2.3316 W ^{-0.8}
91-rod heated section	2.6618 W ^{-0.8}
blanket section	4.7911 W ^{-0.8}
61-rod both sections	3.8293 W ^{-0.8}

Rod section length n

(same as FRS,
Table 3)

^aW is the total bundle mass flow, lb/s.

As noted in the FRS coolant model description, an instantaneous (algebraic) energy balance relationship is appropriate for the gas side:

$$(WC_p)_H (T_{Hi} - T_{Ho}) = (hA)_H (\bar{T}_H - \bar{T}_m) . \quad (21)$$

This reduces to

$$T_{Hi} - T_{Ho} = n_H (\bar{T}_H - \bar{T}_m) , \quad (22)$$

where n_H is referred to as the "section length" for the hot-side gas = $(hA)_H / (WC_p)_H$, dimensionless. Likewise,

$$T_{ci} - T_{co} = n_c (\bar{T}_c - T_T) , \quad (23)$$

where $n_c = (hA)_c / (WC_p)_c$.

The tube lengths in each node are specified to be short enough so that arithmetic-mean temperature differences are sufficiently accurate to predict the heat transfer rates; hence, for the coolant side

$$\bar{T}_c = 0.5 (T_{ci} + T_{co}) . \quad (24)$$

A similar equation applies to the hot side.

As the length of the section increases, n increases as well, and the accuracy of the arithmetic mean approximation worsens. Further, for $n > 2$, the initial response of T_{Ho} to a step change in T_{Hi} will be opposite in sign to the input change. Since this is nonphysical, the heat exchanger models are split up into enough sections so that at minimum expected flow rates, both n_H and $n_c < 2.0$.

The value of n usually increases with decreasing flow rate because h is dependent on W , e.g., if $h \propto W^{0.8}$, then $n \propto W^{0.8} / W^{1.0} = W^{-0.2}$.

In the MACRO model for a typical gas-to-gas heat exchanger section, the mean cool-side gas temperature is determined by combining Eqs. (23) and (24):

$$\bar{T}_c = \frac{T_{ci} + (n_c T_T / 2)}{1.0 + (n_c / 2)} . \quad (25)$$

A similar equation is used for the hot-side gas by substituting subscript H for c.

6.2.2 Initial condition calculations

In a typical simulation run, the initial values of helium inlet and outlet temperatures and flow are specified, along with the ambient air coolant inlet temperature. This requires an initial (steady-state) iterative solution for cooling air flow, and the procedure makes use of the CSMP-III implicit (IMPL) feature and the concept of heat exchanger effectiveness. The cooling effectiveness ϵ_c is defined as

$$\epsilon_c \equiv \frac{T_{Hi} - T_{Ho}}{T_{Hi} - T_{ci}}, \quad (26)$$

where if T_{Ho} were equal to the cooling gas inlet temperature, T_{ci} , the device would be 100% effective ($\epsilon_c = 1.0$). For a counterflow heat exchanger,

$$\epsilon_c = \frac{1 - \exp[-(1-N_1)N_2]}{1 - N_1 \exp[-(1-N_1)N_2]} \quad (27)$$

In terms of the quantities defined previously,

$$N_1 = n_c \tau_c / n_H \tau_H \quad (28)$$

$$N_2 = 12n_H / (1.0 + \tau_c / \tau_H) \quad (29)$$

The reason for the number 12 in Eq. (29) is that the model for the HX-1 uses a 12-section approximation. The iterative solution adjusts values of W_c (accounting for the fact that the crossflow heat transfer coefficient $h_c \propto W_c^{0.6}$) until the above equations and a hot- and cold-side heat balance, i.e.,

$$W_c C_{pc} \Delta T_c = W_H C_{pH} \Delta T_H, \quad (30)$$

are satisfied to within a prescribed accuracy.

6.2.3 Natural convection model

An air-side natural convection flow model for the main heat exchanger HX-1 was developed in order to predict low-flow, low-power loop transients. HX-1 is designed such that natural convection flow is in the same direction as forced convection flow so there will be an orderly transition between the two during transients.

The basic equation used to relate flow and pressure drop is a variation of one derived in ref. 6

$$\Delta P = W^2 \left(\frac{R}{g_c A^2 P} \right) \left[K_i T_i + K_o T_o + T_o - T_i + \frac{2fL}{D} \bar{T} \right] + \frac{gP}{g_c R} \left[\sum_{j=1}^{NR} \frac{L}{\bar{T}_j} + \frac{L_o}{T_o} - \frac{L_i}{T_i} \right], \quad (31)$$

where

- ΔP = total pressure drop, lb_f/ft^2 ,
- W = flow rate, lb_m/sec ,
- R = gas constant for air, $53.3 \text{ ft lb}_f \text{ }^\circ\text{R}^{-1} \text{ lb}^{-1}$,
- g = acceleration due to gravity, 32.2 ft/s^2 ,
- g_c = conversion factor, $32.2 \text{ ft lb}_m \text{ s}^{-2} \text{ lb}_f^{-1}$,
- A = minimum flow area, ft^2 ,
- P = average pressure, lb_f/ft^2 ,
- $K_{i,o}$ = lumped resistance coefficients for inlet and outlet orifices and other restrictions,
- $T_{i,o}$ = inlet, outlet temperatures, $^\circ\text{R}$,
- NR = number of rows of tubes (= 12),
- f = Fanning friction factor,
- L = tube row height, ft,
- L_o = height of outlet column, ft,
- L_i = height of inlet column, ft,
- D = mean hydraulic diameter, ft,
- \bar{T} = average air temperature, $^\circ\text{R}$,
- \bar{T}_j = average temperature, row j , $^\circ\text{R}$.

The temperature difference terms ($T_o - T_i$) account for the losses due to acceleration, and the term on the right-hand side is the buoyancy, or static head term.

The friction factor calculation for the tube bundle (air side) was derived from ref. 7, which uses an experimentally derived factor λ :

$$\lambda = \frac{2\Delta P_g \rho}{4G_m^2 N_r}, \quad (32)$$

where

- ρ = density, lb_m/ft^3 ,
 G = superficial mass velocity through minimum space between tubes, $\text{lb}_m/\text{s ft}^2$,
 N_r = number of rows of tubes, where in this case a "row" is a line of tubes normal to the flow (= 24).

The curve for λ in ref. 7 is approximated by

$$\lambda \approx 0.08(W/W_0)^{-0.29}; \quad (33)$$

at full flow, $W = W_0$, and the Reynolds number is $\sim 25,000$. The factor λ is utilized in the basic flow-pressure drop equation [Eq. (31)] by equating the friction term fL/D to λN_r .

6.3 Circulator and Loop Flow Equations

6.3.1 Circulator flow

The normalized performance map (Fig. 6) was derived from the circulator vendor's map showing head vs flow for various speeds ($N/N_0 = 100, 75, 50,$ and 25%). The resulting curve fit gives approximate values of Y , where

$$Y \approx a_0 + a_1 X + a_2 X^2, \quad (34)$$

for

$$Y = \frac{(\Delta P/\Delta P_0)}{\rho N^2/(\rho N^2)_0}, \quad (35)$$

and

$$X = \frac{W/W_0}{\rho N / (\rho N)_0} . \quad (36)$$

The rms error of the fit was 0.052 (in units of y). Pertinent parameters are:

$$\begin{aligned} \Delta P_0 &= 79.47 \text{ psi,} \\ \rho_0 &= 0.4323 \text{ lb/ft}^3, \\ N_0 &= 1.0 = \text{normalized speed,} \\ W_0 &= 7.0 \text{ lb/s,} \\ a_0 &= 0.9624, \\ a_1 &= 0.70927, \\ a_2 &= 0.720385. \end{aligned}$$

In Fig. 6, at $X=1$, the curve fit gives a value of less than 1 (0.9513) for Y . To adjust for the proper rated conditions, the curve was arbitrarily biased (new $a_0 = 1.0111$) to force it to pass through (1.0,1.0). Also, the surge and full-flow limits correspond to X values of 0.5 and 1.25, respectively, and indicate the recommended method of monitoring these limits during operation; i.e., for given (measured) values of N and ρ , one should ensure that

$$0.5 < W/\rho N < 1.25 . \quad (37)$$

Substitution of Eqs. (35) and (36) into Eq. (34) gives the circulator ΔP as a quadratic function of W :

$$\Delta P_{\text{circ}} = \frac{\Delta P_0 \rho N^2}{(\rho N^2)_0} \left[a_0 + a_1 \frac{1/W_0}{\rho N / (\rho N)_0} W + a_2 \frac{1/W_0^2}{(\rho N)^2 / (\rho N)_0^2} W^2 \right] . \quad (38)$$

As was noted, ORCULT approximates the loop flow resistances by

$$\Delta P_L \approx K_L \left(\frac{\bar{T}}{\bar{P}} \right) W^2 , \quad (39)$$

or

$$\Delta P_L \approx K'_L W^2, \quad (40)$$

where

\bar{T}, \bar{P} = effective absolute temperature and pressure of loop,
 K'_L = a loop resistance parameter that accounts for temperature and pressure variations.

The calculation of K'_L depends on the particular loop configuration and usually involves finding effective flow resistances for several series and parallel paths:

1. For series paths:

$$\Delta P_S = \Delta P_1 + \Delta P_2,$$

$$\Delta P_1 = K'_1 W^2,$$

and

$$\Delta P_2 = K'_2 W^2;$$

thus

$$\Delta P_S = (K'_1 + K'_2)W^2 = K'_S W^2. \quad (41)$$

2. For parallel paths:

$$\Delta P_P = \Delta P_1 = \Delta P_2 = K'_1 W_1^2 = K'_2 W_2^2,$$

and

$$W = W_1 + W_2;$$

thus

$$\Delta P_p = \frac{1}{(1/\sqrt{K_1} + 1/\sqrt{K_2})^2} W^2 = K_p' W^2 . \quad (42)$$

For cases in which a loop component ΔP does not vary as W^2 , the value of K' for that component is adjusted appropriately, as shown in the next section.

For cases not involving a loop depressurization, the solution for circulator flow is found by setting

$$\Delta P_{\text{circ}} = \Delta P_L$$

and solving Eqs. (38) and (40) as a quadratic function of W .

The temperature rise of the gas across the circulator is found from

$$\Delta T_c = k_{cT} \frac{\Delta P_c}{\epsilon_c C_p \rho} , \quad (43)$$

where

- ΔT_c = circulator helium flow temperature rise, °F,
- k_{cT} = conversion constant, $(\text{in.}^2/\text{ft}^2)/(\text{ft lb}_f/\text{Btu}) = 0.186$,
- ΔP_c = circulator ΔP , psi,
- ϵ_c = circulator efficiency = 0.8, dimensionless,
- C_p = gas specific heat, $\text{Btu lb}^{-1} \text{°F}^{-1}$,
- ρ = gas density, lb/ft^3 .

The calculated temperature rise at rated flow conditions is $\sim 34^\circ\text{F}$, which agrees with data obtained from tests of the prototype.

A model is not available for calculating circulator coastdown, and until one is acquired or developed, ORCULT will use arbitrary function fits of manufacturer-supplied curves (Fig. 12). At given loop conditions, such as those specified in Fig. 12, i.e. three circulators on at full speed and a loop pressure of 1300 psia, simulation runs can be made with other initial speeds by starting at the appropriate time value on the graph.

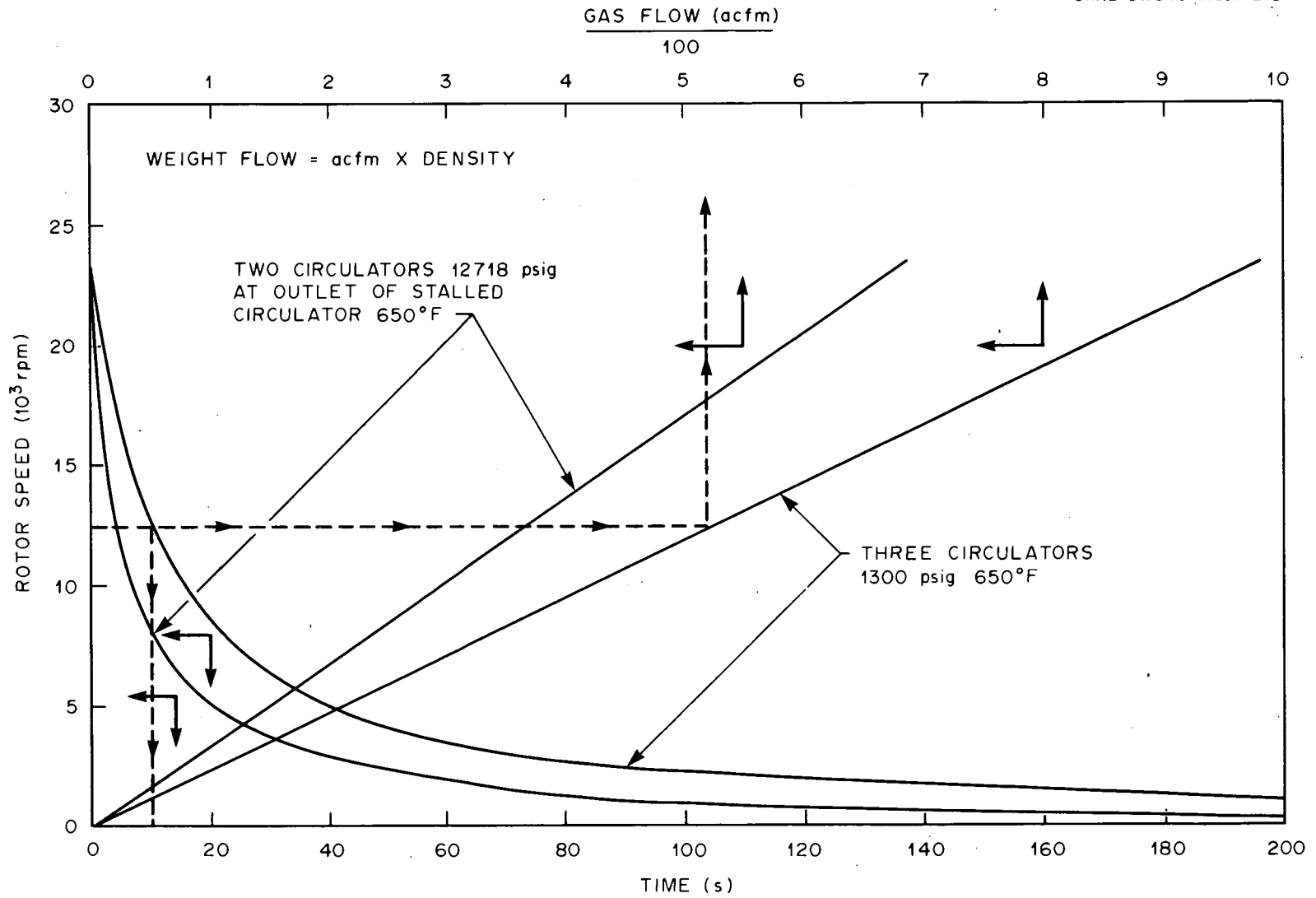


Fig. 12. Circulator coastdown curve at operating pressure.

6.3.2 Loop component flow equations

Loop and component flow resistances are characterized in ORCULT by equations of the form

$$\Delta P = K_L \frac{\bar{T}}{P} W^x . \quad (44)$$

When the flow exponent x is not equal to 2.0, the value of K_L is modified continuously such that ΔP is a function of W^2 , i.e.,

$$K'_L W^2 = K_L W^x ;$$

thus

$$K'_L = K_L W^{(x-2)} . \quad (45)$$

The resistances are lumped together in sections as shown in Fig. 13.

When HX-2 is deleted, resistances KRCF and KRPI are lumped together, and KRH2 is omitted. Although the resistance values designated do not include valve resistances, they do include the nonrecoverable losses from the flow meters. The present reference design includes a venturi meter in the line to the test section, and vortex meters in the attenuator, circulator, and HX-2 lines.

In the present simulation, only the turbulent flow regime is modeled, and the static head or buoyant forces in the loop are neglected.

Expressions for the flow-pressure-drop relations for the various loop components were derived by project personnel and are presented below. Typically they are used in ORCULT in a "lumped" form. For example, the resistance KRH1 (Fig. 13) includes piping, a mixer, and HX-1, all of which have various forms or exponents in their respective flow equations. To lump a composite equation of the form

$$\Delta P = \frac{\bar{T}}{P} (a_1 W^{x1} + a_2 W^{x2} + \dots) , \quad (46)$$

We first compute ΔP for two values of W that span the range of interest.

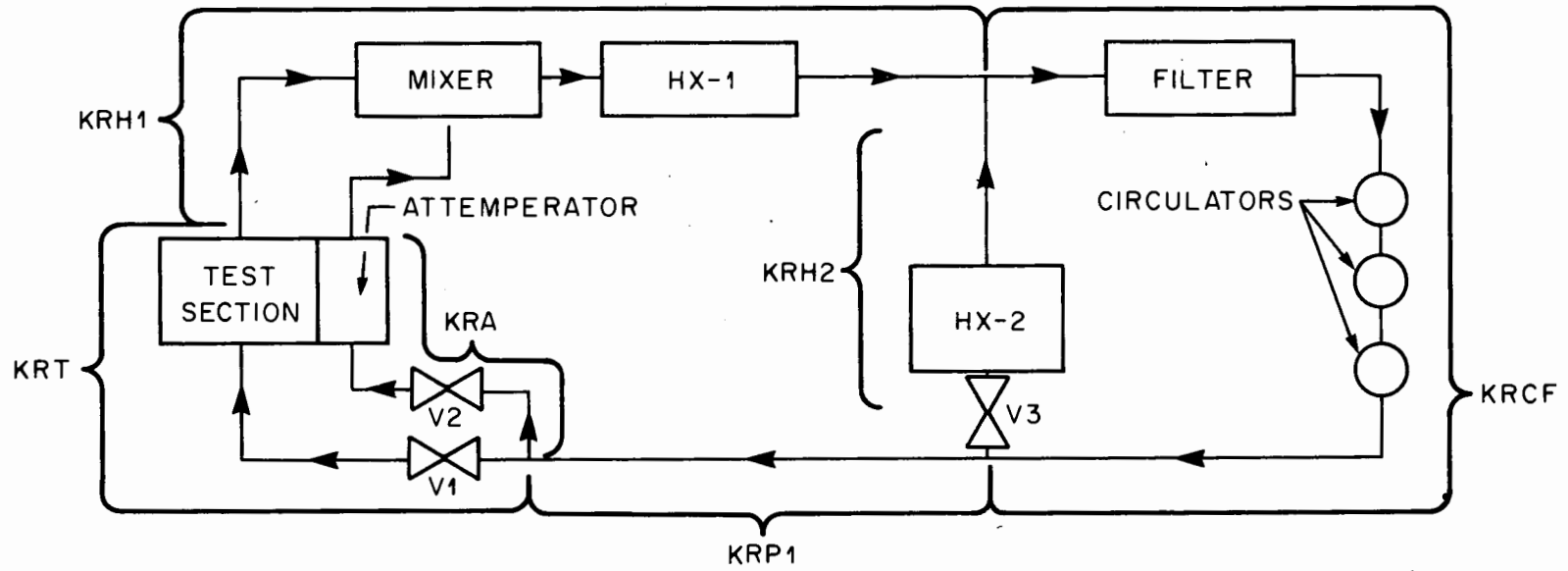


Fig. 13. Loop flow resistance lumping.

A "lumped" exponent value x_L is calculated from

$$\left(\frac{W_1}{W_2}\right)^{x_L} = \frac{\Delta P_1}{\Delta P_2}, \quad (47)$$

and the lumped coefficient a_L can be found once x_L is known, where the lumped version of the equation is

$$\Delta P = a_L \left(\frac{\bar{T}}{\bar{P}}\right) W^{x_L}. \quad (48)$$

Checks of the approximate equation at other values of W are made, and typically show good agreement.

Expressions derived for the test section, including the inlet and outlet nozzles, lead-in piping, and flow meters are

$$\Delta P_{TS} = KRT \left(\frac{\bar{T}}{\bar{P}}\right) W^2, \quad (49)$$

where $KRT = 1.48$ for a 91-rod bundle, and 7.97 for a 37-rod bundle.

Since the calculated pressure drop in the bundle due to acceleration losses (from heating the gas) can be a significant part of the total drop, it is included in ORCULT.

The equation used is similar to that used for the HX-1 natural convection:

$$\Delta P_{\text{accel}} = W^2 \frac{R}{g_c A^2 P} \Delta T, \quad (50)$$

where

- ΔP_{accel} = pressure drop due to acceleration, lb_f/ft^2 ,
- W = bundle mass flow, lb_m/s ,
- R = gas constant for helium,
= $386 \text{ ft lb}_f \text{ }^\circ\text{R}^{-1} \text{ lb}_m^{-1}$,
- g_c = conversion factor, $32.2 \text{ ft lb}_m \text{ s}^{-2} \text{ lb}_f^{-1}$,
- A = bundle flow area, ft^2 ,
- P = average pressure, lb_f/ft^2 ,
- ΔT = temperature rise across bundle, $^\circ\text{R}$.

With a value of 0.03397 ft^2 for A for the new 37-rod bundle,⁵ psi for psf, and the bundle flow area scaled linearly with the number of rods,⁵ Eq. (50) becomes

$$\Delta P_{\text{accel}} = 685.9 \frac{W^2 \Delta T}{P (\text{NRODS})^2} \text{ (psi)} . \quad (51)$$

Information derived from manufacturer's data on the four-element, 6-in.-ID Turbu mixer downstream of the test section gives

$$\Delta P_{\text{mixer}} = 0.085 \left(\frac{T}{P} \right) W^2 , \quad (52)$$

which results in a pressure drop of ~ 4.5 psi at rated conditions and a design flow of $7 \text{ lb}_m/\text{s}$.

The expression for the helium-side pressure drop in HX-1⁸ is a combination of orifice losses proportional to W^2 and friction losses proportional to $W^{1.793}$. The (negative) acceleration losses from cooling the helium are small, and are approximated by factoring a negative loss term into the overall expression. The equation used is

$$\Delta P_{\text{HX-1}} = 0.01268 \left(\frac{T}{P} \right) W^{1.793} = 1.471 \times 10^{-2} \left(\frac{T}{P} \right) W^2 . \quad (53)$$

For design conditions and a loop flow of $7 \text{ lb}_m/\text{s}$, $\Delta P_{\text{HX-1}}$ is ~ 5 psi. The approximate expression for the HX-2 leg pressure drop is

$$\Delta P_{\text{HX-2}} = 1.038 \left(\frac{T}{P} \right) W^{1.83} . \quad (54)$$

The expression used for the maximum pressure drop of the filter is⁹

$$\Delta P_{\text{filter}} = 2.31 \times 10^{-2} \left(\frac{T}{P} \right) W + 4.575 \times 10^{-2} \left(\frac{T}{P} \right) W^{1.83} + 2.227 \times 10^{-2} \left(\frac{T}{P} \right) W^2 . \quad (55)$$

This gives a total pressure drop of ~ 2.4 psi at rated conditions and a design flow of $7 \text{ lb}_m/\text{s}$.

The valve coefficients c_v for the control valves are related to gas mass flow, ΔP , and density by¹⁰

$$W = 0.0176 c_v \sqrt{\rho \Delta P} ; \quad (56)$$

where

ρ = gas density downstream of the valve, lb/ft³,

ΔP = pressure drop across valve, psi,

W = flow through valve, lb/s.

The valve control programs are set up to limit the c_v values to the maximum obtainable. Equal-percentage valve trim characteristics are used, i.e., for a constant ΔP across the valve

$$W/W_{MAX} \propto a e^{by} , \quad (57)$$

where a and b are constants, and y is the normalized valve stem position.

A typical equal-percentage valve trim would give 4% change in (non-sonic) flow (relative to the current operating point value) for a 1% change in stroke (stem position), assuming that ΔP remained constant (in this case, $a = 0.02$ and $b = 3.912$). Because valve position changes in the CFTL result in ΔP changes as well, the valve equations are factored in to the overall loop flow-resistance equations.

Initially, the valve flow and ΔP are given or derived inputs; so the initial value of c_v is obtained from Eq. (56). For a valve with a maximum c_v given, the initial normalized valve position y is found from

$$\frac{c_{vo}}{c_{vMAX}} = \frac{W_o}{W_{MAX}} = 0.02 e^{3.912 y_o} ;$$

then

$$y_o = \frac{1}{3.912} \ln \left(\frac{c_{vo}}{0.02 c_{vMAX}} \right) , \quad (58)$$

and y is limited in the program to values between 0 and 1.

The pressure losses in the piping and fittings are calculated for a given pipe section from

$$\Delta P = 6.0412 \times 10^{-6} \left(\frac{T}{P} \right) \frac{W^{1.83}}{A^2} \left(\frac{L}{D} \right)_{eq}, \quad (59)$$

where

A = pipe flow area, ft^2 ,
 $\left(\frac{L}{D} \right)_{eq}$ = equivalent L/D's of pipe in the section.

Values of effective flow resistance coefficients $\left[6.0412 \times 10^{-6} \left(\frac{L}{D} \right)_{eq} / A^2 \right]$ are shown in Table 5 for various sections of loop piping.

Table 5. Flow resistance values for sections of loop piping

Section	$6.0412 \times 10^{-6} \left(\frac{L}{D} \right)_{eq} / A^2$
Mixer - filter	0.063
Filter - bypass line	0.043
Bypass line - junction of attenuator and test section pipe	0.023
Test section inlet line	0.031
Attenuator inlet line	0.417
HX-2 - bypass line	0.692

Composite values of loop, lumped-section flow resistances and exponents (not including the control valves) are shown in Table 6.

Table 6. Composite flow resistance parameters

Section ^a	Flow Resistance Coeff. K_R	Lumped Exponent Value
KRT - 91-rods	1.48	2.0
KRT - 37-rods	7.97	2.0
KRT - 61-rods	--	2.0
KRA	0.500	1.87
KRH1	0.278	1.9
KRH2	1.038	1.83
KRP1	0.017	2.0
KRCF	0.144	1.85

^aSee Fig. 13.

6.3.3 Loop pressure and internal energy calculations

For cases not involving loop depressurization, loop flows are calculated as algebraic (instantaneous) equation solutions. At the same time, the nominal loop absolute pressure variations with constant loop inventory and varying loop temperatures are calculated by a two-point approximation, where

$$M_T = M_1 + M_2 , \quad (60)$$

and

$$\bar{P} = R \left(\frac{M_1 \bar{T}_1}{V_1} \right) = R \left(\frac{M_2 \bar{T}_2}{V_2} \right) . \quad (61)$$

Solving for \bar{P} from Eqs. (60) and (61) gives

$$\bar{P} = \frac{RM_T}{\frac{V_1}{\bar{T}_1} + \frac{V_2}{\bar{T}_2}} . \quad (62)$$

The node points for \bar{T}_1 and \bar{T}_2 were arbitrarily chosen to be at the circulator outlet and the mixed outlet of the test section. For cases involving changes in loop inventory, the same two points are used as nodes in mass balance equations:

$$\frac{dM_1}{dt} = W_C - W_L - W_D, \quad (63)$$

and

$$\frac{dM_2}{dt} = W_L - W_C, \quad (64)$$

where W_C , W_L , and W_D are the circulator, loop and depressurization flows, respectively.

To account for expansion cooling at the node points during DBDAs, the equations for conservation of total internal energy and mass are used:

$$\frac{dU}{dt} = -hW = -C_p TW \quad (65)$$

and

$$\frac{dM}{dt} = -W, \quad (66)$$

where

- $U = uM =$ total internal energy in node, Btu,
- $u \equiv C_v T =$ specific internal energy, Btu/lb_m,
- $h \equiv C_p T =$ enthalpy, Btu/lb_m,
- $M =$ mass of helium in node, lb_m,
- $W =$ mass flow out of node, lb_m/s,
- $C_v =$ specific heat at constant volume, Btu/lb_m °F,
- $C_p =$ specific heat at constant pressure, Btu/lb_m °F.

Expanding Eqs. (65) and (66) to solve for the node temperatures for net flows in and out (W_{in} , W_{out}) gives

$$\frac{d\bar{T}}{dt} = \frac{\gamma}{M} (T_{in} W_{in} - \bar{T} W_{out}) - \frac{\bar{T}}{M} (W_{in} - W_{out}), \quad (67)$$

where $\gamma \equiv C_p/C_v = 1.67$ for helium.

For the depressurization transients, the coefficients in the equations for W_D are chosen to give near-complete depressurization in a specified time. For the initial (sonic flow) period, we can write

$$P = P_0 e^{-kt}, \quad (68)$$

where P is the loop pressure; P_0 , initial pressure; and t , time.

For an approximate depressurization time T_d to a final (ambient) pressure P_f , the coefficient k is found from

$$e^{-k(T_d)} = P_f/P_0. \quad (69)$$

Hence, the initial values of dP/dt and dM_T/dt are

$$\left. \frac{dP}{dt} \right|_{t=0} = -kP_0 \quad (70)$$

and

$$\left. \frac{dM_T}{dt} \right|_{t=0} = W_{D0} = \left. \frac{dP}{dt} \right|_{t=0} \frac{M_T}{P_0}. \quad (71)$$

Because of the close coupling between the two pressure nodes, this calculation is done on the basis of total average loop pressure P and mass M_T .

For sonic flow

$$W_D = k_s P, \quad (72)$$

where k_s is determined from the initial values of W_D and P . After the

pressure reaches the critical pressure ratio (CPR), where

$$\text{CPR} = \left(\frac{2}{\gamma + 1} \right)^{\frac{\gamma}{\gamma - 1}} = 0.487 \text{ for helium,} \quad (73)$$

then

$$W_D = k_n \sqrt{P^2 - P_f^2}. \quad (74)$$

In Eq. (74), the nonsonic coefficient k_n is approximated by equating the values of W_D at the point where $P = P_f/0.487$.

6.4 Pipe Models

6.4.1 Piping Lag Approximations

The representation of the thermal lags due to heat transfer between a flowing fluid and piping is both important (to CFTL dynamics) and potentially complex (due to the distributed characteristics of long-pipe, low-flow systems). A simplified approximation for insulated long-pipe, variable-flow thermal lags was derived¹¹ which accounts for the mixed high- and low-frequency response nature of the response to a step change in gas temperature into a pipe. The outlet temperature response consists of an immediate output fraction of the input, "THRU," where

$$\text{THRU} = \exp(-n), \quad (75)$$

and the balance of the response is lagged by a time constant τ :

$$\tau \approx \tau_p \exp(0.48 n), \quad (76)$$

where $n = hA/WC_p$, and $\tau_p = MC_p/hA$ (s) are the section length and pipe time constant quantities like those derived for the heat exchanger models.

Thus, the two equations required to approximate the piping thermal lag are

$$T_{go} = T_{gi} \text{ THRU} + (1.0 - \text{THRU}) T_p \quad (77)$$

and

$$\frac{dT_p}{dt} = \frac{1}{\tau} (T_{gi} - T_p) , \quad (78)$$

where T_{gi} and T_{go} are the gas inlet and outlet temperatures, respectively, and T_p is the nominal pipe temperature. The initial value of T_p is set equal to the initial T_{gi} .

The insulated pipe model is implemented in a MACRO called "PIP." A variation of this model, called "PIPL," was developed to simulate piping with significant heat losses. A detailed calculation of heat losses from the piping may include T^4 radiation and nonlinear natural convection effects, and would normally result in a nominal heat-loss value for operating temperatures. PIPL approximates changes in heat loss by a simple linear relation to the initial difference between pipe and ambient temperatures.

In the case of a "lossy" pipe, the initial nominal pipe temperature T_{p0} can be calculated from

$$T_{gi} - \Delta T_{L0} = T_{gi} \text{ THRU} + (1.0 - \text{THRU}) T_{p0} , \quad (79)$$

where

$$\Delta T_{L0} = Q_{L0} / (WC)_{p0} ,$$

The pipe loss time constant τ_L can also be found from a steady-state solution to the lossy pipe equation

$$\frac{dT_p}{dt} = \frac{1}{\tau} (T_{gi} - T_p) + \frac{1}{\tau_L} (T_a - T_p) , \quad (80)$$

where T_a is the ambient temperature.

The pipe sizes, lengths, and model parameters are shown in Table 7.

Table 7. CFTL pipe models

No.	Location	Pipe Size (in., sched.)	Length (ft)	n^a	τ_p^a (s)
0	Test section mixer	10, 160	4.0	0.0804	55.6
1	HX-1 inlet	6, 160	30.0	0.543	50.1
2	HX-1 outlet	6, 80	30.0	0.494	34.7
3	HX-2 inlet and outlet	6, 80	24.75	0.408	34.7
4	Test section inlet	6, 80	27	0.445	34.7
5	Attenuator inlet	6, 80	42	0.692	34.7
6	Circulator inlet (with filter)	6, 80	6.8	0.112	34.7
7	Circulator outlet	6, 80	39.5	0.651	34.7

^aValues shown are for a nominal full-flow value of W ($W = 6.14$ lb/s).

6.4.2 Pipe thermal gradients

The results of calculations of pipe and vessel radial thermal gradients were used as inputs to calculations (by others) of thermal stresses at various points in the loop. Those points included the HX-1 inlet header and first row (hot end) piping, the mixer at the outlet of the test section and the pipe just downstream of the mixer, and the liner and pressure wall in the outlet end of the test section. Thermal gradient calculations for each point were made both for a worst-case DBDA and for a sudden loss of bundle power with full cooling flow maintained.

The fine-structure pipe models were approximated by slab geometry heat diffusion equations (Fig. 14). For a heat transfer area A in the Y-Z plane, NE total nodes with uniform node spacing ΔX , and constant properties k , ρ , and C_p , the equation for the last node (NE) is

$$\rho C_p A \Delta X \frac{dT_{NE}}{dt} = \frac{kA}{\Delta X} (T_{NE-1} - T_{NE}) + \frac{2kA}{\Delta X} (T_S - T_{NE}) . \quad (81)$$

ORNL-DWG 79-17065 ETD

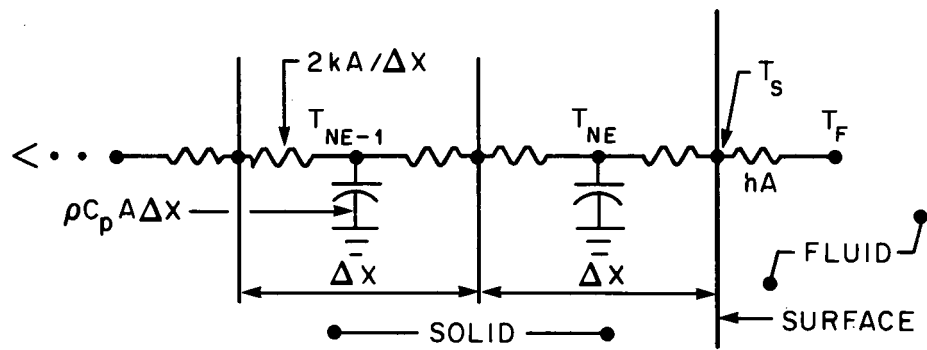


Fig. 14. Slab geometry heat diffusion model.

The surface temperature T_S can be expressed as an instantaneous function of the (forcing function) fluid temperature T_F and T_{NE} :

$$T_S = T_F + (T_{NE} - T_F) \left(\frac{1/h}{\Delta X/2k + 1/h} \right). \quad (82)$$

Noting that the Biot number N_{Bi} and diffusivity α are

$$N_{Bi} = \frac{h\Delta X}{k},$$

and

$$\alpha = \frac{k}{\rho C_p},$$

We can write the expression for the right-hand node T_{NE} (for use in matrix form) as

$$\begin{aligned} \frac{dT_{NE}}{dt} = & \frac{\alpha}{(\Delta X)^2} T_{NE-1} - \frac{\alpha}{(\Delta X)^2} \left[1 + 2 \left(1 - \frac{2}{N_{Bi} + 2} \right) \right] T_{NE} \\ & + \frac{2\alpha}{(\Delta X)^2} \left(1 - \frac{2}{N_{Bi} + 2} \right) T_F. \end{aligned} \quad (83)$$

The expression for each central node T_I is

$$\frac{dT_I}{dt} = \frac{\alpha}{(\Delta X)^2} T_{I-1} - \frac{2\alpha}{(\Delta X)^2} T_I + \frac{\alpha}{(\Delta X)^2} T_{I+1} + Q' \dots, \quad (84)$$

where Q' is an optional heat generation input term (with units of degrees per unit time).

If the left side of the slab is insulated, the expression is

$$\frac{dT_1}{dt} = - \frac{\alpha}{(\Delta X)^2} T_1 + \frac{\alpha}{(\Delta X)^2} T_2 + Q'. \quad (85)$$

Otherwise, with convection heat transfer on the left side, the equation for T_1 would be like Eq. (83) with N_{Bi} modified appropriately.

6.5 Controller Model

The MACRO for a proportional-integral-derivative (PID), three-mode controller has provisions for variable gain and time-constant settings, and built-in gain limits on the integral and derivative stages of 100 and 10, respectively. These limits correspond to nominal values found in typical industrial controllers. The set-point input is designed to enter the calculation downstream of the derivative stage. By changing the sign of the input gain term G , the user can choose to have either an increasing or decreasing output signal with an increasing error signal. Addition of output limits and feedforward signals is left as a user option external to the MACRO.

The frequency domain equation for the integral stage is that of a low-pass filter with a maximum (low-frequency) gain of 100 and a minimum (high-frequency) gain of 1.0. The time constant τ_I of the high-frequency break point is also known as the "reset time," and $1/\tau_I$ is the "reset rate".

$$\left. \frac{X_o}{X_i} \right|_{\text{integral}} = \frac{100 (\tau_I S + 1)}{100 \tau_I S + 1}, \quad (86)$$

where S is the Laplace argument.

The equation for the derivative stage is that of a high-pass filter with a maximum (high-frequency) gain of 10 and a low-frequency gain of 1.0. The time constant of the low-frequency break point, τ_D , is the "derivative time."

$$\left. \frac{X_o}{X_i} \right|_{\text{derivative}} = \frac{\tau_D S + 1}{0.1 \tau_D S + 1}. \quad (87)$$

The proportional stage, with gain = G , simply multiplies the error by G , and the total controller output is the product of all three stages times the error signal.

REFERENCES

1. IBM Application Program: System/360 Continuous System Modeling Program (CSMP) User's Manual, GH20-0367-4 (January 1972).
2. GCFR Prog. Rep. for Period Jan. 1, 1974, to June 30, 1975, ORNL-5119 (June 1976), pp. 83-92.
3. S. J. Ball, "Approximate Models for Distributed Parameter Heat Transfer Systems," Trans. Instrum. Soc. Amer. 3 (1), 38 (January 1964).
4. Letter from H. S. Chung to D. R. Buttemer, "Some Aspects of CACS Characteristics After a Depressurization Accident," Feb. 17, 1976, General Atomic Co. (internal correspondence).
5. Personal communication, J. C. Conklin, August 1979.
6. S. J. Ball, ORECA-I: A Digital Computer Code for Simulating the Dynamics of HTGR Cores for Emergency Cooling Analysis, ORNL/TM-5159 (April 1976).
7. W. H. Giedt, Principles of Engineering Heat Transfer, D. Van Nostrand, Princeton, 1961.
8. Personal communication, W. A. Hartman, July 19, 1978.
9. Personal communication, W. A. Hartman, April 26, 1978.
10. D. M. Considine (ed.), Process Instruments & Controls Handbook, McGraw-Hill, New York, 1957, p. 10-73.
11. S. J. Ball, "Simulation of Plug-Flow Systems," Instrum. Cont. Syst. 36 (2), 133-40 (February 1963).

INTERNAL DISTRIBUTION

- | | | | |
|--------|-----------------|--------|----------------------------|
| 1. | S. M. Babcock | 42-49. | P. R. Kasten |
| 2-21. | S. J. Ball | 50. | A. D. McNutt |
| 22. | R. S. Booth | 51. | L. C. Oakes |
| 23. | N. E. Clapp | 52. | RSIC |
| 24. | W. R. Clark | 53. | A. R. Sadlowe |
| 25. | J. C. Cleveland | 54. | G. S. Sadowski |
| 26. | C. W. Collins | 55. | J. P. Sanders |
| 27. | J. C. Conklin | 56. | J. A. Seneker |
| 28. | T. B. Conley | 57. | R. S. Stone |
| 29. | M. H. Fontana | 58. | H. C. Young |
| 30-34. | U. Gat | 59-60. | Central Research Library |
| 35-37. | A. G. Grindell | 61. | Document Reference Section |
| 38. | W. A. Hartman | 62. | ORNL Patent Office |
| 39. | P. G. Herndon | 63-64. | Laboratory Records |
| 40. | S. A. Hodge | 65. | Laboratory Records-RC |
| 41. | W. R. Huntley | | |

EXTERNAL DISTRIBUTION

- 66-71. DOE, Division of Nuclear Power Development, Washington, DC 20545, Director G. A. Newby, GCFR Branch; L. M. Welshans
- 72-74. Assistant Manager, Energy Research and Development; Director, Nuclear Research and Development Division, DOE, ORO, P.O. Box E, Oak Ridge, TN 37830
- 75-240. DOE, Technical Information Center, P. O. Box 62, Oak Ridge, TN 37830. Given distribution as shown in TID-4500 under category UC-77